

Associated Production of Higgs Bosons and a Photon in High-Energy e^+e^- Collisions

A. DJOUADI*, V. DRIESEN, W. HOLLIK AND J. ROSIEK†

Institut für Theoretische Physik, Universität Karlsruhe,
D-76128 Karlsruhe, FR Germany.

Abstract

We calculate the cross sections for the production of Higgs particles in association with a photon in e^+e^- collisions, $e^+e^- \rightarrow \gamma + \text{Higgs}$, allowing for the longitudinal polarization of the initial electron and positron beams. We consider the associated production of both the Standard Model Higgs boson, and the neutral CP-even and CP-odd Higgs particles of its minimal supersymmetric extension. Complete and compact analytical expressions are given, and the size of the cross sections is illustrated for energies which will be reached at future e^+e^- colliders.

*Supported by Deutsche Forschungsgemeinschaft DFG (Bonn).

†Permanent adress: Institute for Theoretical Physics, Warsaw University, PL-00681 Warsaw, Poland.
Supported by the Alexander von Humboldt Stiftung and by the Polish Committee of Scientific Research.

1. Introduction

The search for Higgs particles and the study of the electroweak symmetry breaking mechanism [1] is one of the most important goals of future high-energy colliders. Once Higgs particles are found, it will be of utmost importance to make a detailed study of their basic properties. In particular, the measurement of the couplings of the Higgs bosons to the other fundamental particles will be a crucial test of the nature of the Higgs bosons. In this respect, future e^+e^- colliders [2] will play a major role: the clean environment in these machines will allow a rather precise determination of these couplings.

In e^+e^- collisions, the couplings of the Standard Model (SM) Higgs boson H^0 to the massive gauge bosons W and Z can be precisely measured in the main production channels: the bremsstrahlung process $e^+e^- \rightarrow H^0 Z$ [3] and the WW/ZZ fusion mechanisms $e^+e^- \rightarrow W^*W^*/Z^*Z^* \rightarrow H^0\bar{\nu}_e\nu_e/H^0e^+e^-$ [4]. The Higgs couplings to fermions can also be measured in some mass range: for Higgs masses below the WW threshold, the strength of the Higgs couplings to τ leptons and charm quarks, relative to the dominant coupling to bottom quarks can be determined [5]. The large Higgs Yukawa coupling to heavy top quarks can be measured in the production process $e^+e^- \rightarrow t\bar{t}H^0$ [6] or if the Higgs is heavy enough to decay into top quarks, in the process $e^+e^- \rightarrow H^0 Z \rightarrow t\bar{t}Z$ [7]. Finally, the trilinear Higgs self-coupling can be accessed via the double Higgs production processes $e^+e^- \rightarrow ZH^0H^0$ and $e^+e^- \rightarrow W^*W^* \rightarrow \bar{\nu}_e\nu_eH^0H^0$ [8].

Another set of important Higgs boson couplings consists of the H^0gg , $H^0\gamma\gamma$ and $H^0Z\gamma$ vertices. These couplings do not occur at the tree level but are induced by loops of heavy particles. Because of the Higgs interaction being proportional to the particle masses, the particles do not decouple for very large masses, and these vertices could therefore serve to count the number of particles which couple to the Higgs boson. The H^0gg vertex [9] can be accessed through the decay $H^0 \rightarrow gg$ in e^+e^- collisions for Higgs bosons in the mass range below ~ 140 GeV, or in the fusion reaction $gg \rightarrow H^0$ which is the main production mechanism of Higgs particles at LHC. The $H^0\gamma\gamma$ and $H^0Z\gamma$ couplings can be accessed in the decays $H^0 \rightarrow \gamma\gamma$ [10, 11] and $H^0 \rightarrow Z\gamma$ [11, 12] which typically have branching ratios of $\mathcal{O}(10^{-3})$ and could be measured at the LHC. The $H^0\gamma\gamma$ width can also be determined directly by means of the $\gamma\gamma$ fusion process [with the photons generated by Compton back-scattering of laser light] at high-energy e^+e^- colliders [13], while the $H^0Z\gamma$ coupling can be measured in the rare decay of the neutral vector boson $Z \rightarrow H^0\gamma$ [11, 14, 15], if H^0 is light enough.

A precise determination of these couplings could help to distinguish between the SM Higgs boson and Higgs particles predicted by some of its extensions such a two-Higgs Doublet Model (2HDM), supersymmetric theories (SUSY) [1] or some other type of New

Physics [16]. For instance, in the Minimal Supersymmetric extension of the Standard Model (MSSM), the Higgs sector is enlarged to contain two doublets of scalar fields leading to a spectrum of five Higgs particles: two CP–even Higgs bosons h and H , a CP–odd Higgs boson A and two charged Higgs particles H^\pm . In the decoupling regime [17], where the Higgs bosons H , A and H^\pm are very heavy, the lightest MSSM Higgs particle h has exactly the properties of the SM Higgs boson, except that its mass is restricted to be smaller than $M_h \lesssim 140$ GeV [18, 19]. If the SUSY particles are too heavy to be produced directly at the colliders, the only way to discriminate between the SM Higgs boson H^0 and h in the decoupling limit is to look at the Higgs couplings to $Z\gamma$ and $\gamma\gamma$. While in the SM these couplings are induced by heavy fermion and W boson loops only, the MSSM provides additional contributions from loops involving charginos and sfermions [20, 21].

An alternative way to have access to these induced Higgs– $\gamma\gamma$ and Higgs– $Z\gamma$ couplings is to consider the process

$$e^+e^- \rightarrow H^0\gamma. \quad (1.1)$$

In the SM, this process proceeds through s –channel $\gamma^*\gamma H^0$ and $Z^*\gamma H^0$ vertex diagrams, but additional t –channel vertex and box diagrams involving W /neutrino and Z /electron exchange also occur (Fig. 1a). This process has been discussed some time ago in Ref. [22] and more recently in Ref. [23] for unpolarized electron and positron beams. Since it is a higher–order process in the electroweak coupling¹, the cross section is rather small, but the signal is very clean allowing for a reasonable hope to isolate these events [25] if enough luminosity is collected at a future high–energy collider.

In this paper, we rederive the cross section for the process eq. (1.1) in the Standard Model, but allowing for the longitudinal polarization of the initial e^+ and e^- beams. In addition, we consider the associated production of a photon and a Higgs boson in supersymmetric theories. In the MSSM, the associated production of the CP–even neutral Higgs particles

$$\begin{aligned} e^+e^- &\rightarrow h\gamma \\ e^+e^- &\rightarrow H\gamma \end{aligned} \quad (1.2)$$

and the production of the CP–odd Higgs boson

$$e^+e^- \rightarrow A\gamma \quad (1.3)$$

will receive additional contributions coming from SUSY loops. For the CP–even Higgs bosons one has additional s –channel γ, Z exchange vertex diagrams involving loops with

¹A similar process is the loop induced double production of Higgs particles, $e^+e^- \rightarrow \Phi\Phi$, which has been discussed in the SM and the MSSM recently [24].

charged Higgs bosons, charginos, squarks and sleptons as well as t -channel vertex and box diagrams involving chargino/sneutrino and neutralino/selectron loops (Fig. 1b). For the pseudoscalar state A , because of CP invariance, the process is mediated only by s -channel vertex diagrams involving chargino and fermion loops, as well as t -channel vertex and box diagrams involving chargino/sneutrino and neutralino/selectron loops (Fig. 1c).

The rest of the paper is organized as follows. In the next section, we analyze the associated Higgs-photon production in the Standard Model. In section 3, the case of the neutral CP-even and CP-odd Higgs bosons of the minimal supersymmetric extension is discussed. Some additional technical material is given in a short Appendix.

2. Associated $H\gamma$ production in the SM

2.1 Decomposition into form factors

In the Standard Model, the process $e^+e^- \rightarrow \gamma H^0$ is described to lowest order by the Feynman diagrams depicted in Fig. 1a. There are s -channel γ and Z exchange vertex diagrams involving virtual W and heavy fermion loops [mainly top and bottom quark loops, since the Yukawa couplings to the light fermions are very small], as well as t -channel vertex diagrams involving W /neutrino and Z /electron exchanges [corrections to the $H^0 ee$ vertex] and W /neutrino and Z /electron box diagrams. Additional contributions come from diagrams where the Higgs boson is emitted from the virtual Z line and with Z - γ mixing through fermion or W boson loops; diagrams with the mixing between the Z boson (or the photon) and the Higgs boson give negligible contributions.

Allowing for the polarization of both the initial electron and positron beams, and summing over the polarizations of the photon, the differential cross section of the process can be written as

$$\frac{d\sigma}{d\cos\theta}(e^+e^- \rightarrow \gamma H^0) = \frac{1}{2s} \frac{s - M_H^2}{16\pi s} \sum_{\text{pol}} |\mathcal{M}|^2 \quad (2.1)$$

where \sqrt{s} is the c.m. energy and θ the scattering angle of the photon. Neglecting the electron mass, the amplitude \mathcal{M} can be decomposed into the following sum of amplitudes

$$\mathcal{M} = \sum_{i=1,3} \sum_{v=+,-} \Lambda_i^v C_i^v \quad (2.2)$$

where the form factors C_i^\pm sum all diagrams of Fig. 1a:

$$C_i^\pm = C_i^{\gamma^\pm} + C_i^{Z^\pm} + C_i^{e^\pm} + C_i^{\text{box}^\pm} . \quad (2.3)$$

C^γ and C^Z denote the contributions of the γ and Z pole vertex diagrams, C^e the t -channel $H^0 ee$ vertex corrections and C^{box} the contributions of the box diagrams; the contributions due to the Z - γ mixing are included in C^Z . Denoting by p_\pm the momentum [all momenta are taking to be incoming] of the initial e^\pm beams, p_γ and ϵ_γ the photon momentum and polarization vector, the set of standard matrix elements Λ_i^\pm is given by

$$\begin{aligned}\Lambda_1^\pm &= \bar{v}(p_+) (1 \pm \gamma_5) (\not{\epsilon}_\gamma p_\gamma \cdot p_- - \not{p}_\gamma \epsilon_\gamma \cdot p_-) u(p_-) \\ \Lambda_2^\pm &= \bar{v}(p_+) (1 \pm \gamma_5) (\not{\epsilon}_\gamma p_\gamma \cdot p_+ - \not{p}_\gamma \epsilon_\gamma \cdot p_+) u(p_-) \\ \Lambda_3^\pm &= \bar{v}(p_+) (1 \pm \gamma_5) (\not{\epsilon}_\gamma) u(p_-) .\end{aligned}\tag{2.4}$$

Summing over the photon polarizations, the squared amplitude can be written as

$$\sum_{\text{pol}} |\mathcal{M}|^2 = \frac{1}{(16\pi^2)^2} \left[\sum_{v=+,-} \sum_{i,j=1,3} C_i^v T_{ij}^{vv} (C_j^v)^* \right] \tag{2.5}$$

with

$$\begin{aligned}T_{ij}^{++} &= \sum_{\text{pol}} \Lambda_i^+ (\Lambda_j^+)^{\dagger} = \frac{1}{4} (1 + \lambda_-) (1 - \lambda_+) T_{ij} \\ T_{ij}^{--} &= \sum_{\text{pol}} \Lambda_i^- (\Lambda_j^-)^{\dagger} = \frac{1}{4} (1 - \lambda_-) (1 + \lambda_+) T_{ij} \\ T_{ij}^{-+} &= T_{ij}^{+-} = 0\end{aligned}\tag{2.6}$$

where λ_- and λ_+ are the longitudinal polarizations of the initial e^- and e^+ beams, respectively. In terms of the usual Mandelstam variables $s = (p_- + p_+)^2$, $u = (p_- + p_\gamma)^2$ and $t = (p_+ + p_\gamma)^2$, the matrix T reads

$$T_{ij} = 2s \begin{pmatrix} u^2 & 0 & 2u \\ 0 & t^2 & 2t \\ 2u & 2t & 4 \end{pmatrix} . \tag{2.7}$$

In fact, as we will discuss later in more details, QED gauge invariance requires that the form factors C_3^\pm vanish after summing over the contributions of all Feynman diagrams. This is obvious from eq. (2.4): while the form factors $\Lambda_{1,2}^\pm$ vanish if the polarization of the photon ϵ_γ is replaced by its momentum p_γ , it is not the case for Λ_3^\pm ; the transversality of the photon therefore implies that it is the amplitude C_3^\pm which should vanish. Therefore, one can drop the contributions of Λ_3^\pm and the differential cross section of the process $e^+ e^- \rightarrow \gamma H^0$ can be written in the simple form

$$\begin{aligned}\frac{d\sigma}{d\cos\theta} &= \frac{s - M_H^2}{64\pi s} \frac{1}{(16\pi^2)^2} \left\{ (1 + \lambda_-) (1 - \lambda_+) \left[u^2 |C_1^+|^2 + t^2 |C_2^+|^2 \right] \right. \\ &\quad \left. + (1 - \lambda_-) (1 + \lambda_+) \left[u^2 |C_1^-|^2 + t^2 |C_2^-|^2 \right] \right\} ,\end{aligned}\tag{2.8}$$

where the scattering angle θ is related to t by $t = -(s - M_H^2)(1 - \cos \theta)/2$. The unpolarized cross section is obtained by simply setting $\lambda_{\pm} = 0$:

$$\frac{d\sigma^{\text{unpol.}}}{d\cos\theta} = \frac{s - M_H^2}{64s\pi} \frac{1}{(16\pi^2)^2} \left[u^2 (|C_1^+|^2 + |C_1^-|^2) + t^2 (|C_2^+|^2 + |C_2^-|^2) \right]. \quad (2.9)$$

2.2 s -channel diagrams

Let us now discuss the contributions of the various diagrams to the form factors C_i^{\pm} and start with the s -channel vertex and Z -photon mixing contributions. The contributions of the fermions and W bosons to the $\gamma\gamma H^0$ or $Z\gamma H^0$ vertex diagrams can be decomposed into the following tensorial form [all momenta are taken as incoming and $V \equiv Z, \gamma$]:

$$\begin{aligned} \Gamma[V^{\mu}(p_V), \gamma^{\nu}(p_{\gamma}), H^0(p_H)] = & G_1^V g^{\mu\nu} + G_2^V p_{\gamma}^{\mu} p_{\gamma}^{\nu} + G_3^V p_{\gamma}^{\mu} p_V^{\nu} + G_4^V p_V^{\mu} p_{\gamma}^{\nu} \\ & + G_5^V p_V^{\mu} p_V^{\nu} + G_6^V \epsilon^{\mu\nu\alpha\beta} p_{V\alpha} p_{\gamma\beta} \end{aligned} \quad (2.10)$$

Neglecting the electron mass, for on-shell final photons only the form factors G_1 and G_3 contribute to the amplitude. They are related to the form factors $C_{1,2}^{Z,\gamma}$ by

$$\begin{aligned} C_1^{\gamma\pm} &= C_2^{\gamma\pm} = -\frac{e}{2} \frac{1}{s} G_3^{\gamma} \\ C_1^{Z\pm} &= C_2^{Z\pm} = -\frac{e z^{\pm}}{4s_W c_W} \frac{1}{s - M_Z^2} G_3^Z \end{aligned} \quad (2.11)$$

where e is the electric charge, $z^+ = -1 + 2s_W^2$ and $z^- = 2s_W^2$ with $s_W^2 = 1 - c_W^2 \equiv \sin^2 \theta_W$. Although only the form factors $C_{1,2}^{Z,\gamma}$ contribute to the $e^+e^- \rightarrow H^0\gamma$ cross section, we also give the expressions for $C_3^{Z,\gamma}$ to check explicitly that QED gauge invariance is indeed fulfilled:

$$\begin{aligned} C_3^{\gamma\pm} &= \frac{e}{2} \frac{1}{s} \left[G_1^{\gamma} - \frac{s - M_H^2}{2} G_3^{\gamma} \right] \\ C_3^{Z\pm} &= \frac{e z^{\pm}}{4s_W c_W} \frac{1}{s - M_Z^2} \left[G_1^Z - \frac{s - M_H^2}{2} G_3^Z \right]. \end{aligned} \quad (2.12)$$

Note that in the previous expressions we have omitted the finite width in the Z boson propagator for simplicity.

The form factors $G_i^{\gamma,Z}$ are obtained by summing bosonic and fermionic contributions to the $V\gamma H^0$ vertices:

$$\begin{aligned} G_i^{\gamma} &= \frac{e^3 M_W}{s_W} \left[F_i^{\gamma,W} - \sum_f 4Q_f^2 N_c \frac{m_f^2}{M_W^2} F_i^f \right] \\ G_i^Z &= \frac{e^3 M_W}{c_W s_W^2} \left[F_i^{Z,W} + \sum_f 2Q_f N_c \frac{m_f^2}{M_W^2} (I_3^f - 2s_W^2 Q_f) F_i^f \right] \end{aligned} \quad (2.13)$$

where Q_f , I_3^f and m_f are the electric charge, weak isospin and mass of the fermion f [in practice only top and bottom quarks] respectively, and N_c is the color factor, $N_c = 1$ for leptons and $N_c = 3$ for quarks.

The explicit calculation of the form factors $G_{1,3}^{\gamma,Z}$ was done in the Feynman gauge where the W boson contributions can be split into the $g^{\mu\nu}$ and charged Goldstone parts. The ultraviolet divergent amplitudes have been reduced from a complicated tensorial form to scalar Passarino-Veltman two- and three-point functions [26] using the package FORM [27]. These scalar functions are defined in the Appendix and their complete analytical expressions can be found in Ref. [28] for instance; their numerical evaluation has been performed using the package FF [29].

The fermion loops give the same contribution $F_{1,3}^f$ to the $\gamma^*\gamma H^0$ and $Z^*\gamma H^0$ vertices since the difference due to the different $\gamma f f$ and $Z f f$ couplings has been factorized out in eq. (2.13):

$$\begin{aligned} F_1^f &= \frac{1}{2} \left[1 + (2m_f^2 - M_H^2 - s)C_0 - 2s(2C_{11} + C_{21}) + 2(s - M_H^2)(C_{12} + C_{23}) \right] \\ F_3^f &= C_0 + 4C_{12} + 4C_{23} \end{aligned} \quad (2.14)$$

with the C_0 and C_{ij} three-point functions defined as

$$C_{ij} \equiv C_{ij}(s, 0, M_H^2; m_f^2, m_f^2, m_f^2) . \quad (2.15)$$

Note that the fermionic contribution to the Z - γ mixing diagrams is proportional to the final photon momentum squared and therefore vanishes for photons on the mass shell.

The W boson loops involving true vertex diagrams [with the exchange of W bosons, charged Goldstones and ghosts] and two-point functions [involving the quartic couplings between two scalars and two vectors] give different contributions to the $\gamma^*\gamma H^0$ and $Z^*\gamma H$ vertices because of the complicated structure of the trilinear gauge boson and quartic gauge boson scalar couplings which are different for the Z and the photon. Summing over all diagrams, the W boson contribution reads

$$\begin{aligned} F_1^{\gamma,W} &= \left(\frac{M_H^2}{M_W^2} + 6 \right) (4C_{24} - B_{13}) + M_H^2(-7C_0 + C_{11} + C_{12}) \\ &\quad + s(5C_0 + C_{11} - C_{12}) - B_{12} + B_{23} \\ F_3^{\gamma,W} &= 4 \left(\frac{M_H^2}{M_W^2} + 6 \right) (C_{12} + C_{23}) + 16C_0 \end{aligned} \quad (2.16)$$

for the $\gamma^*\gamma H^0$ vertex, and

$$F_1^{Z,W} = \frac{1}{2} \frac{M_H^2}{M_W^2} (1 - 2c_W^2) (4C_{24} - B_{13}) + M_H^2 c_W^2 (7C_0 - C_{11} - C_{12} - 2C_{23})$$

$$\begin{aligned}
& +M_H^2(-C_0 + C_{11} - C_{23}) + 2M_W^2(c_W^2 - 1)C_0 \\
& -c_W^2 [s(5C_0 + C_{11} - C_{12} + 2C_{21} - 2C_{23}) + 32C_{24} - B_{12} - 6B_{13} - B_{23}] \\
& +\frac{1}{2} + c_W^2 + s(C_0 - C_{11} - C_{21} + C_{23}) - B_{12} + B_{23} \\
F_3^{Z,W} = & 2 \left[\frac{M_H^2}{M_W^2} (1 - 2c_W^2) + 2(1 - 6c_W^2) \right] (C_{12} + C_{23}) + 4(1 - 4c_W^2)C_0
\end{aligned} \tag{2.17}$$

for the $Z^*\gamma H^0$ vertex. The two-point and three-point functions, B_{ij} [note that here, the B_{ij} functions are different from the standard ones given in [26] for instance] C_{ij} are defined as

$$\begin{aligned}
B_{12} & \equiv B_0(s; M_W^2, M_W^2) \\
B_{13} & \equiv B_0(M_H^2; M_W^2, M_W^2) \\
B_{23} & \equiv B_0(0; M_W^2, M_W^2) \\
C_{ij} & \equiv C_{ij}(s, 0, M_H^2; M_W^2, M_W^2, M_W^2)
\end{aligned} \tag{2.18}$$

The expressions in eq. (2.17) include the W boson contribution to the Z - γ mixing diagrams, which is non-zero only in the case of the form factor $F_1^{Z,W}$ and reads

$$F_1^{Z,W}|_{\text{mix}} = 2B_{23} = 2B_0(0; M_W^2, M_W^2) . \tag{2.19}$$

Finally, we note that while the fermionic contributions are gauge invariant by themselves, i.e. that one has $C_3^\gamma + C_3^Z \equiv 0$ for fermions, the W contributions are not. Gauge invariance of the W contributions is obtained only when the t -channel vertex and the box diagrams are included.

2.3 t -channel vertex and box diagrams

The contributions of the t -channel $H^0 e^+ e^-$ vertex corrections come from W /neutrino and Z /electron loops. Only the “transverse” part of the gauge bosons contribute since the longitudinal or Goldstone part is proportional to the very small electron mass. The contribution of these diagrams to the form factors C_i^e can be written as

$$C_i^{e\pm} = \frac{e^4}{s_W^3} \left[\frac{M_W}{2} A_i^{W\pm} + \frac{M_Z}{4c_W^3} A_i^{Z\pm} \right] + \text{crossed} \tag{2.20}$$

with the W /neutrino contributions

$$\begin{aligned}
A_3^{W+} & = C_{12}(m_e^2, t, M_H^2; M_W^2, 0, M_W^2) \\
A_3^{W-} & = 0 \\
A_1^{W\pm} & = A_2^{W\pm} = 0
\end{aligned} \tag{2.21}$$

and the Z /electron contributions

$$\begin{aligned} A_3^{Z\pm} &= (z^\pm)^2 C_{12}(m_e^2, t, M_H^2; M_Z^2, m_e^2, M_Z^2) \\ A_1^{Z\pm} &= A_2^{Z\pm} = 0 . \end{aligned} \quad (2.22)$$

The crossed terms are obtained by substituting $t \rightarrow u$ in the functions C_{12} of eqs. (2.21) and (2.22). Because of the t -channel electron exchange, terms proportional to $\ln(m_e^2)$ appear and one therefore has to keep a finite value for the electron mass in the argument of the C_{12} functions. This dependence on $\ln(m_e)$ will disappear after adding the W and Z box contributions.

Finally, the contribution of the box W and Z diagrams to the form factors C_i^{box} can be written as

$$C_i^{\text{box}\pm} = -\frac{e^4 M_W}{4 s_W^3} [B_i^{W\pm} + \text{crossed}] + \frac{e^4 M_Z}{4 s_W^3 c_W^3} B_i^{Z\pm} . \quad (2.23)$$

The terms from the W /neutrino box contribution read:

$$\begin{aligned} B_1^{W+} &= 4(D_0 + D_{11} - D_{13} + D_{23} - D_{25}) \\ B_2^{W+} &= 4(-D_{12} + D_{13} + D_{23} - D_{26}) \\ B_3^{W+} &= \frac{1}{2} [3s(-D_{12} + D_{13} + D_{25} + D_{26} - D_{23} - D_{24}) \\ &\quad + 7t(-D_{23} + D_{26}) + u(3D_{13} + 7D_{25} - 7D_{23}) - 20D_{27}] . \end{aligned} \quad (2.24)$$

Since the W boson is left-handed, there is no contribution from the W boxes to the form factors B_i^{W-} :

$$B_{1,2,3}^{W-} = 0 . \quad (2.25)$$

The four-point functions D_0 and D_{ij} have to be understood as

$$D_{ij} = D_{ij}(m_e^2, m_e^2, M_H^2, 0, s, u; M_W^2, 0, M_W^2, M_W^2) \quad (2.26)$$

in the expressions given above, while in the crossed contributions one has to interchange the photon and Higgs boson masses and interchange $u \leftrightarrow t$ in eqs. (2.24) and (2.26)

$$D_{ij} = D_{ij}(m_e^2, m_e^2, 0, M_H^2, s, t; M_W^2, 0, M_W^2, M_W^2) . \quad (2.27)$$

The Z /electron box contributions in eq. (2.23) are given by

$$\begin{aligned} B_1^{Z\pm} &= 2(z^\pm)^2 (-D_{11} + D_{12} + D_{22} - D_{24}) \\ B_2^{Z\pm} &= 2(z^\pm)^2 (D_{22} - D_{26}) \\ B_3^{Z\pm} &= (z^\pm)^2 [s(D_{22} - D_{24} + D_{25} - D_{26}) + 2D_{27}] \end{aligned} \quad (2.28)$$

where

$$D_{ij} = D_{ij}(m_e^2, M_H^2, m_e^2, 0, t, u; M_Z^2, m_e^2, m_e^2, M_Z^2) . \quad (2.29)$$

There is no crossed contribution here since the photon does not couple to the Z boson directly. Again, we have kept the electron mass in the arguments of the functions D_{ij} to avoid infrared singularities; these logarithmic singularities cancel exactly, as it should be, those which appear in the t -channel $H^0 ee$ vertex contributions.

2.4 Results

We have verified explicitly that the sum of the W and the Z boson contributions from the various diagrams is gauge invariant, i.e. that the form factor C_3 in eq. (2.3) indeed vanishes when all contributions are added. This cancellation occurs as follows: the Z /electron contributions to the $H^0 ee$ vertex and the box diagrams cancel each other, $C_3^{e\pm} + C_3^{\text{box}\pm} = 0$. Furthermore, the W boson contributions to $C_3^{\gamma-} + C_3^{Z-}$ is zero, and as discussed previously the contributions to C_i^- of the W boson induced $H^0 e^+ e^-$ vertex and box diagrams are zero since the W boson is left-handed. Finally, the form factor C_3^+ vanishes after summing the W boson contributions of all diagrams. This feature, together with the fact that the sum of all contributions is both ultraviolet and infrared finite, provides a very strong check of the calculation.

We have also compared our results with previous calculations of the $e^+ e^- \rightarrow H^0 \gamma$ cross section in the unpolarized case [22, 23]. Our analytical results agree completely with the results² of Ref. [23], provided that their fermionic contribution to the s -channel $\gamma^* \gamma H^0$ and $Z \gamma H^0$ vertices is multiplied by a factor of two. Our result for the fermionic contributions agrees with the one obtained in Ref. [11, 15, 14] for the $Z \rightarrow H^0 \gamma$ decay and also with Ref. [22] if the color factor for quarks is included in the fermionic sum. We have also compared numerically our results with those of Ref. [22], who calculated the $e^+ e^- \rightarrow H^0 \gamma$ cross section using the Feynman gauge. Our numbers agree with those given in Tab. 4 of Ref. [22] up to a few percent; the small difference is probably due to a slightly different choice of input parameter values.

The cross sections for the process $e^+ e^- \rightarrow H^0 \gamma$ are shown in Fig. 2 as a function of the Higgs boson mass for two center of mass energies $\sqrt{s} = 500$ GeV and 1.5 TeV typical of future high-energy $e^+ e^-$ colliders. At 500 GeV, the unpolarized cross section [solid curve] is of the order of $\sigma \sim 0.05$ fb for light Higgs masses and increases slightly when

²The results of Ref. [23] have been obtained using a non-linear gauge and the individual contributions are therefore different from ours; however the sum of all contributions is gauge invariant and can be compared with our final result.

approaching the WW threshold; it then drops out quickly with increasing M_H due to the lack of phase space. At $\sqrt{s} = 1.5$ TeV, the cross section for light H^0 drops by a factor of ~ 5 compared to the previous case, but the decrease with increasing M_H is slower.

Fig. 2 shows also the effect on the cross section of polarizing longitudinally the electron and positron beams. With left-handed longitudinally polarized electrons [dashed lines] the cross section $\sigma(e_L^- e^+ \rightarrow H^0 \gamma)$ is approximately two times larger, and with left-handed electrons and right-handed positrons [dotted lines] the cross section $\sigma(e_L^- e_R^+ \rightarrow H^0 \gamma)$ is approximately four times larger than in the unpolarized case. The longitudinal polarization of both the electron and positron beams is therefore important to increase the cross section; for energies in the 300 GeV range the cross section can reach values of the order of 0.5 fb for $M_H \sim 100$ GeV.

Fig. 3a exhibits the dependence of the cross section on the center of mass energy for several values of the Higgs boson mass. The cross section increases rapidly with the opening of the phase space and then decreases near $\sqrt{s} \sim 350$ GeV close to the $t\bar{t}$ threshold [the W and top quark contributions interfere destructively, and the top contribution is maximal near the $t\bar{t}$ threshold]. The cross section drops smoothly with increasing energy; despite of the presence of t -channel vertex and box contributions, it scales approximately as $1/s$ at high energies. For $M_H \sim 100$ GeV, the cross section can be maximized by running the collider at energies around 250 GeV.

Finally, Fig. 3b shows the angular distribution $d\sigma/d\cos\theta$ for a c.m. energy of 500 GeV and a Higgs boson mass $M_H = 100$ GeV. The distribution is forward-backward symmetric and does not depend very strongly on the Higgs boson mass.

With the yearly integrated luminosity of $\mathcal{L} \sim 100 \text{ fb}^{-1}$ expected at future high-energy e^+e^- colliders, one could collect a few tens of $H^0\gamma$ events in the course of a few years, if longitudinal polarization is available³. The signal, which mainly consists of a photon and a $b\bar{b}$ pair in the low Higgs mass range or WW and ZZ pairs for Higgs masses larger than ~ 160 GeV, is extremely clean. The backgrounds should be very small since the photon must be very energetic and the $b\bar{b}$ or WW/ZZ pairs should peak at an invariant mass M_H [these rare events will be searched only once the Higgs boson is found in one of the main production channels and the Higgs mass would be precisely known by then]. Therefore, despite of the low rates, the clean signal gives a reasonable hope to isolate these events.

³Note that at the CERN collider LEP2 with a c.m. energy of $\sqrt{s} \sim 180$ GeV, the expected luminosity which will be available, $\mathcal{L} \sim 0.5 \text{ fb}^{-1}$, does not allow to produce any $H^0\gamma$ event.

3. Associated production of MSSM Higgs bosons

In the MSSM, the associated production of the CP-even Higgs bosons h, H and the CP-odd Higgs boson A with a photon receives extra contributions from loops involving charged Higgs bosons and genuine supersymmetric particles. More precisely, the production of the CP-even Higgs particles, $e^+e^- \rightarrow \Phi\gamma$ with $\Phi = h, H$, proceeds through the same diagrams as for the SM Higgs boson substituting the Higgs couplings to W, Z bosons and fermions, plus those of Fig. 1b: (i) s -channel γ, Z exchange vertex diagrams involving loops built up by charged Higgs boson, chargino, squark and slepton loops, (ii) t -channel diagrams correcting the Φee vertex involving chargino/sneutrino and neutralino/selectron loops, and (iii) box diagrams involving chargino/sneutrino and neutralino/selectron states.

For the associated production of the pseudoscalar state A , because of CP invariance, there is no contribution from W/Z bosons, charged Higgs bosons and sfermions in the vertex diagrams and no contribution from W/Z bosons in the box diagrams. The process $e^+e^- \rightarrow A\gamma$ is therefore mediated only by s -channel vertex diagrams involving chargino and fermion loops, as well as t -channel vertex and box diagrams involving chargino/sneutrino and neutralino/selectron states (Fig. 1c).

The differential cross section for $e^+e^- \rightarrow \Phi\gamma$ with $\Phi = h, H$ and A is given by the same formulae as in the SM, eq. (2.1), with M_H replaced by M_Φ . Again, since by virtue of gauge invariance the form factor C_3^\pm vanishes, the cross section with polarized e^+e^- beams reduces as in eq. (2.8) to

$$\begin{aligned} \frac{d\sigma}{d\cos\theta} = & \frac{s - M_\Phi^2}{64s\pi} \frac{1}{(16\pi^2)^2} \left\{ (1 + \lambda_-)(1 - \lambda_+) \left[u^2 |C_1^+|^2 + t^2 |C_2^+|^2 \right] \right. \\ & \left. + (1 - \lambda_-)(1 + \lambda_+) \left[u^2 |C_1^-|^2 + t^2 |C_2^-|^2 \right] \right\}. \end{aligned} \quad (3.1)$$

In spite of this, we give C_3^\pm to explicitly check gauge invariance. The form factors $C_{1,2}^\pm$ and C_3^\pm are different for the production of CP-even and CP-odd Higgs production. We therefore discuss these two cases separately.

3.1. CP-even Higgs boson production

A. s -channel vertex corrections

The one-loop $\gamma\gamma\Phi$ or $Z\gamma\Phi$ induced vertices can be written in the same tensorial form as in eq. (2.10). For the CP-even Higgs particles, the form factors C_i^\pm are given in terms of the amplitudes G_i^\pm as in the SM by eqs.(2.11–2.12). In the MSSM, the various loop

contributions to the form factors G_i^\pm are given by

$$\begin{aligned}
G_i^\gamma &= \frac{e^3 M_W}{s_W} \left[F_i^{\gamma, W} + F_i^{\gamma, H^+} - \sum_f 4Q_f^2 N_c \frac{m_f^2}{M_W^2} F_i^f \right] + \frac{e^3}{s_W} \left[F_i^{\gamma, \chi^+} + \sum_{\tilde{f}} N_c Q_f F_i^{\gamma, \tilde{f}} \right] \\
G_i^Z &= -\frac{e^3 M_W}{c_W s_W^2} \left[F_i^{Z, W} + F_i^{Z, H^+} - \sum_f 2Q_f N_c \frac{m_f^2}{M_W^2} (I_3^f - 2s_W^2 Q_f) F_i^f \right] \\
&\quad - \frac{e^3}{s_W} \left[F_i^{Z, \chi^+} + \sum_{\tilde{f}} N_c Q_f F_i^{Z, \tilde{f}} \right], \tag{3.2}
\end{aligned}$$

where $F_i^{V, W}$, F_i^{V, H^+} , F_i^{V, χ^+} , $F_i^{V, \tilde{f}}$ and F_i^f denote the W boson, the charged Higgs boson, the chargino, the sfermion and the fermion contributions, respectively. Note that while the contributions of the fermions, charged Higgs bosons, charginos and sfermions are separately gauge invariant, the contributions of the W bosons are not [as in the SM] and the contributions of the t -channel vertex and box diagrams are needed to insure the gauge invariance of this subset of diagrams. The contributions of the various loops are as follows:

W boson loops:

The contributions of the W bosons to the $\gamma^* \gamma \Phi$ vertex are

$$\begin{aligned}
F_1^{\gamma, W} &= g_{\Phi G^+ G^-} \frac{1}{c_W^2} \left[M_W^2 C_0 - 4C_{24} + B_{13} \right] + g_{\Phi V V} \left[M_\Phi^2 (-6C_0 + C_{11} + C_{12}) \right. \\
&\quad \left. + s(5C_0 + C_{11} - C_{12}) + 24C_{24} - B_{12} - 6B_{13} + B_{23} \right] \\
F_3^{\gamma, W} &= -\frac{1}{c_W^2} g_{\Phi G^+ G^-} 4(C_{12} + C_{23}) + g_{\Phi V V} 8(2C_0 + 3(C_{12} + C_{23})) \tag{3.3}
\end{aligned}$$

and the contributions to the $Z^* \gamma \Phi$ vertex are

$$\begin{aligned}
F_1^{Z, W} &= g_{\Phi V V} \left[M_\Phi^2 c_W^2 (-6C_0 + C_{11} + C_{12} + 2C_{23}) + M_\Phi^2 (-C_{11} + C_{23}) \right. \\
&\quad \left. + 2M_W^2 (1 - c_W^2) C_0 + c_W^2 (-1 + s(5C_0 + C_{11} - C_{12} + 2C_{21} - 2C_{23}) + 32C_{24} \right. \\
&\quad \left. - B_{12} - 6B_{13} - B_{23}) - 1/2 - sC_0 + sC_{11} + sC_{21} - sC_{23} + B_{12} - B_{23} \right] \\
&\quad + g_{\Phi G^+ G^-} \left[M_W^2 (1 - c_W^{-2}) C_0 + (1 - c_W^{-2}/2)(4C_{24} - B_{13}) \right] \\
F_3^{Z, W} &= g_{\Phi V V} 4 \left[(4c_W^2 - 1) C_0 + (6c_W^2 - 1)(C_{12} + C_{23}) \right] \\
&\quad + g_{\Phi G^+ G^-} 2 \left[(c_W^{-2} - 2)(C_{12} + C_{23}) \right]. \tag{3.4}
\end{aligned}$$

Note that the bosonic (W, G^+) two-point function contribution to photon- Z boson mixing, $F_1^{Z, W}|_{\text{mix}} = 2B_{23} g_{\Phi V V}$ is included. The two- and three-point functions B and C are

the same as in eq. (2.18) with $M_H \rightarrow M_\Phi$.

At first sight, the couplings of the Higgs bosons to vector bosons and charged Goldstones, which are given in Tab. 1a, look quite different. However, in the MSSM the two couplings are intimately related; for instance in the case of the light CP-even Higgs boson [a similar identity holds for the heavy CP-even Higgs boson], one can write⁴ these couplings in terms of the ratios $r_h = M_h^2/M_Z^2$ and $r_H = M_H^2/M_Z^2$ [1]

$$\begin{aligned} g_{hVV} &\equiv \sin(\beta - \alpha) = \left[\frac{r_H(r_H - 1)}{(r_H - r_h)(r_H + r_h - 1)} \right]^{1/2} \\ g_{hG^+G^-} &\equiv \cos 2\beta \times \sin(\beta + \alpha) = - \left[\frac{r_h r_H}{r_H + r_h - 1} \right]^{1/2} \times \left[\frac{r_h(r_H - 1)}{r_H - r_h} \right]^{1/2} \end{aligned} \quad (3.5)$$

and therefore

$$\frac{g_{hG^+G^-}}{g_{hVV}} = - \frac{M_h^2}{M_Z^2}. \quad (3.6)$$

Inserting this identity, which is also valid in an arbitrary two-Higgs Doublet Model (see for example [30]), in eqs. (3.3–3.4), one then recovers the standard W boson contributions eqs. (2.16–2.17) with an overall additional factor $g_{\Phi VV}$.

Fermion loops:

The contributions of the fermion loops are as in the SM, modulo a global factor $g_{\Phi ff}$ for the couplings of the Higgs bosons to fermions relative to the SM Higgs couplings (see Tab. 1b):

$$\begin{aligned} F_1^f &= \frac{g_{\Phi ff}}{2} \left[1 + (2m_f^2 - M_\Phi^2 - s)C_0 - 2s(2C_{11} + C_{21}) + 2(s - M_\Phi^2)(C_{12} + C_{23}) \right] \\ F_3^f &= g_{\Phi ff} [C_0 + 4C_{12} + 4C_{23}] \end{aligned} \quad (3.7)$$

The three-point functions C_0 , C_{ij} are defined as in eq. (2.15) with $M_H \rightarrow M_\Phi$.

Charged Higgs boson loops:

The contributions of the charged Higgs bosons to the $\gamma\gamma\Phi$ and $Z\gamma\Phi$ vertices are the same as those of the charged Goldstones, and read

$$\begin{aligned} F_1^{\gamma, H^+} &= \left(\frac{1}{c_W^2} g_{\Phi H^+ H^-} + 2g_{\Phi VV} \right) (4C_{24} - B_{13}) \\ F_3^{\gamma, H^+} &= \left(\frac{1}{c_W^2} g_{\Phi H^+ H^-} + 2g_{\Phi VV} \right) 4(C_{12} + C_{23}) \end{aligned} \quad (3.8)$$

⁴These expressions are valid only at the tree-level, however the ratio should not be altered by the radiative corrections in the Higgs sector if the latter are consistently included in both the Higgs boson masses, the mixing angle α and in the trilinear $g_{hG^+G^-}$ coupling.

$$\begin{aligned}
F_1^{Z,H^+} &= \frac{1}{2}(2c_W^2 - 1) \left[2g_{\Phi VV} + \frac{1}{c_W^2} g_{\Phi H^+ H^-} \right] (4C_{24} - B_{13}) \\
F_3^{Z,H^+} &= \frac{1}{2}(2c_W^2 - 1) \left[2g_{\Phi VV} + \frac{1}{c_W^2} g_{\Phi H^+ H^-} \right] 4(C_{12} + C_{23}) .
\end{aligned} \tag{3.9}$$

The couplings $g_{\Phi H^+ H^-}$ are the same as the charged Goldstone couplings $g_{\Phi G^+ G^-}$ given in Tab. 1a at the tree level; however, if the radiative corrections to the Higgs boson masses are incorporated, one should also use the corrected coupling $g_{\Phi H^+ H^-}$ given (3.51), to insure the gauge invariance of the result. The two- and three point functions are defined in this case as

$$\begin{aligned}
B_{13} &= B_0(M_\Phi^2; M_{H^\pm}^2, M_{H^\pm}^2) \\
C_{ij} &= C_{ij}(s, 0, M_\Phi^2; M_{H^\pm}^2, M_{H^\pm}^2, M_{H^\pm}^2) .
\end{aligned} \tag{3.10}$$

Chargino loops:

The chargino contributions F_i^{V,χ^+} with $i = 1, 3$ to the $V\gamma\Phi$ vertices can be cast into the compact form

$$\begin{aligned}
F_i^{V,\chi^+} &= - \sum_{j,k=1,2} \left[f_i(-m_{\chi_j^+}, -m_{\chi_k^+}, -m_{\chi_k^+}) + g_i(-m_{\chi_k^+}, -m_{\chi_j^+}, -m_{\chi_j^+}) \right] \\
&\times \sum_{A,B=L,R} g_{V\chi_j^+ \chi_k^-}^A g_{\Phi\chi_k^+ \chi_j^-}^B .
\end{aligned} \tag{3.11}$$

The couplings of the charginos to the Higgs bosons are given in Tab. 1c, while the chargino couplings to the photon and the Z boson read

$$g_{\gamma\chi_j^+ \chi_k^-}^{L/R} = -\delta_{jk} \quad \text{and} \quad g_{Z\chi_j^+ \chi_k^-}^{L/R} = O'^{L/R}/(s_W c_W) . \tag{3.12}$$

The matrices $O'^{L/R}$ are defined as

$$O'_{ij}^L = -V_{i1}V_{j1}^* - \frac{1}{2}V_{i2}V_{j2}^* + \delta_{ij}s_W^2 \quad , \quad O'_{ij}^R = -U_{i1}U_{j1}^* - \frac{1}{2}U_{i2}U_{j2}^* + \delta_{ij}s_W^2 \tag{3.13}$$

where the U and V matrices which diagonalize the chargino mass matrix can be found in Ref. [31]. The functions $f_i/g_i \equiv f_i/g_i(m_1, m_2, m_3)$ are:

$$\begin{aligned}
f_1 &= m_1 \left[2m_2 m_3 C_0 - M_\Phi^2 (C_0 + C_{11} + 2C_{12} + 2C_{23}) \right. \\
&\quad \left. - s(C_0 + 3C_{11} - 2C_{12} + 2C_{21} - 2C_{23}) - 4C_{24} + 1 \right] \\
g_1 &= m_2 \left[M_\Phi^2 (C_{11} + C_{12} + 2C_{23}) + s(C_{11} - C_{12} + 2C_{21} - 2C_{23}) + 8C_{24} - 1 \right] \\
&\quad + m_3 \left[-M_\Phi^2 (C_{12} + 2C_{23}) - s(2C_{11} - C_{12} + 2C_{21} - 2C_{23}) - 4C_{24} + 1 \right] \\
f_3 &= 2m_1 [C_0 + C_{11} + 2C_{12} + 2C_{23}] \\
g_3 &= 2 \left[-m_2 (C_{11} - C_{12}) + m_3 (C_{12} + 2C_{23}) \right]
\end{aligned} \tag{3.14}$$

The arguments of the three-point functions C_0 and C_{ij} are specified according to

$$C_{ij} = C_{ij}(s, 0, M_\Phi^2; m_{\chi^+}^2, m_{\chi^+}^2, m_{\chi^+}^2) . \quad (3.15)$$

Sfermion loops:

Finally, the squark/slepton contribution to the $V\gamma\Phi$ vertices can be written as

$$F_i^{V,\tilde{f}} = \sum_{j,k=1,2} g_{\Phi\tilde{f}_j\tilde{f}_k} g_{V\tilde{f}_k\tilde{f}_j} s_i \quad (3.16)$$

This term comes only from Higgs emission from the sfermion lines since the contributions of the two- and one-point $Z\text{--}\gamma$ mixing diagrams cancel each other. The functions $s_i \equiv s_i(m_{\tilde{f}_j}, m_{\tilde{f}_k}, m_{\tilde{f}_k})$ read:

$$\begin{aligned} s_1 &= 2B_0(M_\Phi^2; m_{\tilde{f}_k}^2, m_{\tilde{f}_k}^2) - 8C_{24}(s, 0, M_\Phi^2; m_{\tilde{f}_j}^2, m_{\tilde{f}_k}^2, m_{\tilde{f}_k}^2) \\ s_3 &= -8[C_{12}(s, 0, M_\Phi^2; m_{\tilde{f}_j}^2, m_{\tilde{f}_k}^2, m_{\tilde{f}_k}^2) + C_{23}(s, 0, M_\Phi^2; m_{\tilde{f}_j}^2, m_{\tilde{f}_k}^2, m_{\tilde{f}_k}^2)] . \end{aligned} \quad (3.17)$$

The squark couplings to the Higgs bosons, including mixing [32] between left- and right-handed sfermions⁵ are

$$\begin{aligned} g_{\Phi\tilde{f}_1\tilde{f}_1} &= C_{LL}^\Phi \cos^2 \theta_f + C_{RR}^\Phi \sin^2 \theta_f + 2C_{RL}^\Phi \cos \theta_f \sin \theta_f \\ g_{\Phi\tilde{f}_2\tilde{f}_2} &= C_{RR}^\Phi \cos^2 \theta_f + C_{LL}^\Phi \sin^2 \theta_f - 2C_{RL}^\Phi \cos \theta_f \sin \theta_f \\ g_{\Phi\tilde{f}_1\tilde{f}_2} &= C_{RL}^\Phi (\cos^2 \theta_f - \sin^2 \theta_f) + (C_{RR}^\Phi - C_{LL}^\Phi) \cos \theta_f \sin \theta_f \end{aligned} \quad (3.18)$$

with

$$\begin{aligned} C_{LL}^\Phi &= -\frac{M_Z}{c_W} (I_3^f - Q_f s_W^2) g_2^\Phi - \frac{m_f^2}{M_W} g_1^\Phi \\ C_{RR}^\Phi &= -\frac{M_Z}{c_W} (Q_f s_W^2) g_2^\Phi - \frac{m_f^2}{M_W} g_1^\Phi \\ C_{RL}^\Phi &= -\frac{m_f}{2M_W} [A_f g_4^\Phi + \mu g_3^\Phi] , \end{aligned} \quad (3.19)$$

where A_f and μ are the soft-SUSY breaking trilinear term and the Higgs-higgsino mass parameter, respectively. The factors g_i^Φ are given in Tab. 2a, and in the limit of zero-mixing the couplings reduce to those given in Tab. 2b. The photon coupling to sfermions

⁵This mixing is proportional to the fermion mass and in practice, is non negligible only for the partners of the third generation fermions.

is just $g_{\gamma\tilde{f}_i\tilde{f}_j} = \delta_{ij}Q_f$, while the couplings of the Z boson to sfermions in the case of mixing are given by

$$\begin{aligned} g_{Z\tilde{f}_1\tilde{f}_1} &= D_{LL} \cos^2 \theta_f + D_{RR} \sin^2 \theta_f \\ g_{Z\tilde{f}_2\tilde{f}_2} &= D_{RR} \cos^2 \theta_f + D_{LL} \sin^2 \theta_f \\ g_{Z\tilde{f}_1\tilde{f}_2} &= (D_{RR} - D_{LL}) \sin \theta_f \cos \theta_f \end{aligned} \quad (3.20)$$

with

$$D_{LL} = \frac{1}{s_W c_W} (I_3^f - Q_f s_W^2) \quad \text{and} \quad D_{RR} = \frac{1}{s_W c_W} (-Q_f s_W^2) . \quad (3.21)$$

B. t -channel vertex corrections

In addition to the contribution of the W/ν and Z/e SM like loops, there are two additional contributions to the t -channel Φee vertex diagrams: one with chargino/sneutrino loops and another one with neutralino/stop squark loops. In the case where the mixing in the selectron sector is neglected, all these diagrams do not contribute to the form factors $C_{1,2}^{e\pm}$:

$$C_{1,2}^{e\pm} = 0 . \quad (3.22)$$

There is, however, a contribution to the form factors C_3^\pm which reads

$$\begin{aligned} C_3^{e+} &= \frac{e^4}{s_W^3} \left[\frac{M_W}{2} g_{\Phi V V} f_3^{fVV}(M_W, 0, M_W) - \frac{M_Z}{4c_W^3} g_{\Phi V V} (z^+)^2 f_3^{fVV}(M_Z, m_e, M_Z) \right. \\ &\quad + \sum_{A=R,L} \sum_{j,k} g_{e\chi_j^+\nu} g_{e\chi_k^+\nu} g_{\Phi\chi_j^+\chi_k^-}^A f_{3A}^{ffS}(-m_{\chi_j^+}, m_{\tilde{\nu}}, -m_{\chi_k^+}) \\ &\quad - \frac{M_Z}{2c_W} \sum_j g_{e\chi_j^+\nu} g_{e\chi_j^+\nu} g_{\Phi\tilde{\nu}\tilde{\nu}} f_3^{fSS}(m_{\tilde{\nu}}, -m_{\chi_j^+}, m_{\tilde{\nu}}) \\ &\quad + \frac{1}{2} \sum_{A=R,L} \sum_{j,k} g_{e\chi_j^0\tilde{e}_L} g_{e\chi_k^0\tilde{e}_L} g_{\Phi\chi_j^0\chi_k^0}^A f_{3A}^{ffS}(m_{\chi_j^0}, m_{\tilde{e}_L}, m_{\chi_k^0}) \\ &\quad \left. + \frac{M_Z}{4c_W} \sum_j g_{e\chi_j^0\tilde{e}_L} g_{e\chi_j^0\tilde{e}_L} g_{\Phi\tilde{e}_L\tilde{e}_L} f_3^{fSS}(m_{\tilde{e}_L}, m_{\chi_j^0}, m_{\tilde{e}_L}) \right] + \text{crossed} \quad (3.23) \end{aligned}$$

$$\begin{aligned} C_3^{e-} &= \frac{e^4}{s_W^3} \left[-\frac{M_Z}{4c_W^3} g_{\Phi V V} (z^-)^2 f_3^{fVV}(M_Z, m_e, M_Z) \right. \\ &\quad + \frac{1}{2} \sum_{A=R,L} \sum_{j,k} g_{e\chi_j^0\tilde{e}_R} g_{e\chi_k^0\tilde{e}_R} g_{\Phi\chi_j^0\chi_k^0}^A f_{3A}^{ffS}(m_{\chi_j^0}, m_{\tilde{e}_R}, m_{\chi_k^0}) \\ &\quad \left. + \frac{M_Z}{4c_W} \sum_j g_{e\chi_j^0\tilde{e}_R} g_{e\chi_j^0\tilde{e}_R} g_{\Phi\tilde{e}_R\tilde{e}_R} f_3^{fSS}(m_{\tilde{e}_R}, m_{\chi_j^0}, m_{\tilde{e}_R}) \right] + \text{crossed} \quad (3.24) \end{aligned}$$

with $\bar{A} = L, R$ when $A = R, L$ and with the functions $f_{3\cdots} \equiv f_{3\cdots}(m_1, m_2, m_3)$ given by

$$\begin{aligned} f_3^{fSS} &= -\frac{1}{2}C_{12} \\ f_3^{fVV} &= C_{12} \\ f_{3L}^{ffS} &= \frac{1}{2}m_3C_{12} \\ f_{3R}^{ffS} &= \frac{1}{2}m_1(C_0 + C_{12}) \end{aligned} \quad (3.25)$$

involving the three-point functions C_{ij} specified as

$$C_{ij} = C_{ij}(m_e^2, t, M_\Phi^2; m_1^2, m_2^2, m_3^2) \quad (3.26)$$

for the direct diagrams; for the crossed diagrams one has to make the substitution $t \rightarrow u$ in the previous equation. The couplings of the Higgs bosons to vector bosons, charginos and neutralinos are given in Tab. 1, and those to sleptons in Tab. 2b. The only remaining couplings to be defined are the electron–chargino–sneutrino and electron–neutralino–selectron couplings; normalized to $g_W = [\sqrt{2}G_F]^{1/2} M_W$, they are given by

$$g_{e\chi_i^+\tilde{\nu}} = V_{i1} \quad , \quad g_{e\chi_i^0\tilde{e}_R} = 2\frac{s_W}{c_W}N_{i2} \quad , \quad g_{e\chi_i^0\tilde{e}_L} = -N_{i2} - \frac{s_W}{c_W}N_{i1} \quad . \quad (3.27)$$

The matrices V and N which diagonalize the chargino and neutralino mass matrices can be found in Ref. [31].

C. Box corrections

The box diagrams involve the contributions from W /neutrino and Z /electron loops as in the case of the SM Higgs boson, plus chargino/sneutrino and neutralino/selectron loops. The contributions to $C_i^{\text{box}\pm}$ read:

$$\begin{aligned} C_i^{\text{box}+} &= \frac{e^4}{s_W^3} \left[-\frac{M_W}{2} f_i^{fVVV}(M_W, 0, M_W, M_W) - \frac{M_W}{2} f_i^{fVVS}(M_W, 0, M_W, M_W) \right. \\ &\quad + \sum_j \frac{M_Z}{4c_W} g_{e\chi_j^0\tilde{e}_L} g_{e\chi_j^0\tilde{e}_L} g_{\Phi\tilde{e}_L\tilde{e}_L} f_i^{fSSS}(m_{\tilde{e}_L}, m_{\chi_j^0}, m_{\tilde{e}_L}, m_{\tilde{e}_L}) \\ &\quad - \sum_{A=R,L} \sum_{j,k} g_{e\chi_j^+\tilde{\nu}} g_{e\chi_k^+\tilde{\nu}} g_{\Phi\chi_j^+\chi_k^-}^A f_{iA}^{ffffS}(-m_{\chi_j^+}, m_{\tilde{\nu}}, -m_{\chi_k^+}, -m_{\chi_j^+}) \left. \right] + \text{cros.} \\ &\quad + \frac{e^4}{s_W^3} \left[-\frac{M_Z}{4c_W^3}(z^+) f_i^{fVVV}(m_e, M_Z, M_Z, m_e) \right. \\ &\quad + \sum_{A=R,L} \sum_{j,k} \frac{1}{2} g_{e\chi_j^0\tilde{e}_L} g_{e\chi_k^0\tilde{e}_L} g_{\Phi\chi_j^0\chi_k^0}^A g_{iA}^{ffSS}(m_{\chi_j^0}, m_{\tilde{e}_L}, m_{\tilde{e}_L}, m_{\chi_k^0}) \end{aligned}$$

$$\begin{aligned}
& + \sum_{j,k} \frac{M_Z}{2c_W} g_{e\chi_j^+\tilde{\nu}} g_{e\chi_k^+\tilde{\nu}} g_{\Phi\tilde{\nu}\tilde{\nu}} f_i^{ffSS}(-m_{\chi_j^+}, m_{\tilde{\nu}}, m_{\tilde{\nu}}, -m_{\chi_k^+}) \Big] \\
C_i^{\text{box-}} &= \frac{e^4}{s_W^3} \left[\sum_j \frac{M_Z}{4c_W} g_{e\chi_j^0\tilde{e}_R} g_{e\chi_j^0\tilde{e}_R} g_{\Phi\tilde{e}_R\tilde{e}_R} f_i^{fSSS}(m_{\tilde{e}_R}, m_{\chi_j^0}, m_{\tilde{e}_R}, m_{\tilde{e}_R}) \right] + \text{cros.} \\
& + \frac{e^4}{s_W^3} \left[-\frac{M_Z}{4c_W^3} (z^-) f_i^{ffVV}(m_e, M_Z, M_Z, m_e) \right. \\
& \left. + \sum_{A=R,L} \sum_{j,k} g_{e\chi_j^0\tilde{e}_R} g_{e\chi_j^0\tilde{e}_R} g_{\Phi\chi_j^0\chi_k^0}^A g_{i\tilde{A}}^{ffSS}(m_{\chi_j^0}, m_{\tilde{e}_R}, m_{\tilde{e}_R}, m_{\chi_k^0}) \right] \quad (3.28)
\end{aligned}$$

where the sums run over the two chargino and the four neutralino states. All the couplings have been previously defined, and the box functions $f_i^{fxyz} = f_i^{fxyz}(m_1^2, m_2^2, m_3^2, m_4^2)$ are given by

$$\begin{aligned}
f_1^{fSSS} &= -D_{23} + D_{25} \\
f_2^{fSSS} &= -D_{23} + D_{26} \\
f_3^{fSSS} &= \frac{1}{2}[t(D_{23} - D_{26}) + u(D_{23} - D_{25}) + 2D_{27}] \quad (3.29)
\end{aligned}$$

$$\begin{aligned}
f_1^{fVVS} &= 2(D_0 + D_{11}) \\
f_2^{fVVS} &= 0 \\
f_3^{fVVS} &= \frac{1}{2}[-2u(D_0 + D_{11}) - (s + 2t)D_{12} + (s + 2t + u)D_{13} + (s + t + u)D_{23} \\
& \quad + sD_{24} - (s + u)D_{25} - (s + t)D_{26} + 4D_{27}] \quad (3.30)
\end{aligned}$$

$$\begin{aligned}
f_1^{fVVV} &= D_0 + D_{11} - 2D_{13} + 2D_{23} - 2D_{25} \\
f_2^{fVVV} &= 2[-D_{12} + D_{13} + D_{23} - D_{26}] \\
f_3^{fVVV} &= \frac{1}{2}[u(D_0 + D_{11}) - (s - t)D_{12} + (s - t + u)D_{13} - 2(s + 2t + 2u)D_{23} \\
& \quad - 2sD_{24} + 2(s + 2u)D_{25} + 2(s + 2t)D_{26} - 12D_{27}] \quad (3.31)
\end{aligned}$$

$$\begin{aligned}
f_{1L}^{ffffS} &= -m_1(D_0 + D_{11}) + m_4(D_{13} - D_{23} + D_{25}) \\
f_{1R}^{ffffS} &= m_3(-D_{23} + D_{25}) \\
f_{2L}^{ffffS} &= m_4(-D_{23} + D_{26}) \\
f_{2R}^{ffffS} &= m_3(D_{12} - D_{13} - D_{23} + D_{26}) \\
f_{3L}^{ffffS} &= \frac{1}{2}[(m_1 - m_4)sD_{12} - (m_1 - m_4)sD_{13} + (m_1(s + u + t) - m_4s)D_{23} \\
& \quad + (m_1 - m_4)sD_{24} - ((m_1 - m_4)s + m_1u)D_{25} \\
& \quad - ((m_1 - m_4)s + m_1t)D_{26} + (4m_1 - 2m_4)D_{27}] \\
f_{3R}^{ffffS} &= \frac{1}{2}m_3(m_1m_4D_0 - s(D_{23} + D_{24} - D_{25} - D_{26}) - 2D_{27}) \quad (3.32)
\end{aligned}$$

with the four-point functions

$$D_{ij} = D_{ij}(m_e^2, m_e^2, M_\Phi^2, 0, s, u; m_1^2, m_2^2, m_3^2, m_4^2) . \quad (3.33)$$

The remaining box functions read

$$\begin{aligned} f_1^{ffVV} &= 2(-D_{11} + D_{12} + D_{22} - D_{24}) \\ f_2^{ffVV} &= 2(D_{22} - D_{26}) \\ f_3^{ffVV} &= -m_1 m_4 D_0 + s(D_{22} - D_{24} + D_{25} - D_{26}) + 2D_{27} \end{aligned} \quad (3.34)$$

$$\begin{aligned} f_1^{ffSS} &= -D_{22} + D_{24} \\ f_2^{ffSS} &= -D_{12} + D_{13} - D_{22} + D_{26} \\ f_3^{ffSS} &= \frac{1}{2}[m_1 m_4 D_0 - s(D_{22} - D_{24} + D_{25} - D_{26}) - 2D_{27}] \end{aligned} \quad (3.35)$$

with the four-point functions

$$D_{ij} = D_{ij}(m_e^2, M_\Phi^2, m_e^2, 0, t, u; m_1^2, m_2^2, m_3^2, m_4^2) , \quad (3.36)$$

and

$$\begin{aligned} g_{1L}^{ffSS} &= m_1(D_0 + D_{11} + D_{12} + D_{24}) \\ g_{1R}^{ffSS} &= m_4(D_{12} + D_{24}) \\ g_{2L}^{ffSS} &= m_1(D_{13} + D_{26}) \\ g_{2R}^{ffSS} &= m_4(D_{26}) \\ g_{3L}^{ffSS} &= \frac{1}{2}m_1(-u(D_0 + D_{11} + D_{12} + D_{24}) - t(D_{13} + D_{26}) - 2D_{27}) \\ g_{3R}^{ffSS} &= \frac{1}{2}m_4(-u(D_{12} + D_{24}) - tD_{26} - 2D_{27}) \end{aligned} \quad (3.37)$$

with

$$D_{ij} = D_{ij}(m_e^2, 0, m_e^2, M_\Phi^2, u, t; m_1^2, m_2^2, m_3^2, m_4^2) . \quad (3.38)$$

The contribution of the crossed diagrams can be obtained by simply interchanging $t \leftrightarrow u$ in the relevant expressions given above.

The gauge invariance of the complete result has been checked explicitly. The sum of W /neutrino and Z /electron contributions to the t -channel vertex and box diagrams and the contributions of the W bosons to the s -channel vertices are gauge invariant as in the SM. For the neutralino/selectron and the chargino/sneutrino contributions, only the sum $C^e + C^{\text{box}}$ is gauge invariant.

3.2. CP-odd Higgs production

In the case of the CP-odd Higgs bosons, fewer diagrams contribute to the associated production with a photon compared to the case of the CP-even Higgs particles. Indeed, because of CP invariance, there is no pseudoscalar couplings to vector bosons, to charged Higgs bosons and to the SUSY partners of the light fermions. The mixing between left-handed and right-handed third generation sfermions will induce a $A\tilde{f}_1\tilde{f}_2$ coupling, however, CP-invariance still imposes the sum of all sfermion loops to vanish.

A. s -channel vertex corrections

The one-loop $\gamma\gamma A$ or $Z\gamma A$ vertices can be written in the same tensorial form as in eq. (2.10). However, for the CP-odd Higgs boson, the form factors $C_{1,2}^\pm$ are different because now the amplitude G_6 gives a non-vanishing contribution. Using the same notation as previously, we have for the $Z\gamma A$ vertex

$$\begin{aligned} C_1^{Z\pm} &= \frac{e z^\pm}{4c_W s_W} \frac{1}{s - M_Z^2} (-G_3^Z \pm G_6^Z) \\ C_2^{Z\pm} &= \frac{e z^\pm}{4c_W s_W} \frac{1}{s - M_Z^2} (-G_3^Z \mp G_6^Z) \\ C_3^{Z\pm} &= \frac{e z^\pm}{4c_W s_W} \frac{1}{s - M_Z^2} \left(G_1^Z - \frac{s - M_H^2}{2} G_3^Z \right), \end{aligned} \quad (3.39)$$

and for the $\gamma\gamma A$ vertex

$$\begin{aligned} C_1^{\gamma\pm} &= \frac{e}{2} \frac{1}{s} (-G_3^\gamma \pm G_6^\gamma) \\ C_2^{\gamma\pm} &= \frac{e}{2} \frac{1}{s} (-G_3^\gamma \mp G_6^\gamma) \\ C_3^{\gamma\pm} &= \frac{e}{2} \frac{1}{s} \left(G_1^\gamma - \frac{s - M_H^2}{2} G_3^\gamma \right). \end{aligned} \quad (3.40)$$

Only heavy fermion and chargino loops contribute to the form factors G_i^γ and G_i^Z . They are separately gauge invariant and are decomposed according to

$$\begin{aligned} G_i^\gamma &= -\frac{e^3 M_W}{s_W} \sum_f 4Q_f^2 N_c \frac{m_f^2}{M_W^2} F_i^f + \frac{e^3}{s_W} F_i^{\gamma, \chi^+} \\ G_i^Z &= \frac{e^3 M_W}{c_W s_W^2} \sum_f 2Q_f N_c \frac{m_f^2}{M_W^2} (I_3^f - 2s_W^2 Q_f) F_i^f \Big] - \frac{e^3}{s_W} F_i^{Z, \chi^+}. \end{aligned} \quad (3.41)$$

The fermion loop contribution to the $V A \gamma$ vertex F_i^f is given by

$$\begin{aligned} F_1^f &= F_3^f = 0 \\ F_6^f &= -g_{Aff} C_0(s, 0, M_A^2; m_f^2, m_f^2, m_f^2) \end{aligned} \quad (3.42)$$

with the couplings g_{Aff} in Tab. 1a. The chargino loops yield

$$\begin{aligned}
F_{1,3}^{V,\chi^+} &= - \sum_{j,k=1,2} \left[f_{1,3}(-m_{\chi_j^+}, -m_{\chi_k^+}, -m_{\chi_k^+}) + g_{1,3}(-m_{\chi_k^+}, -m_{\chi_j^+}, -m_{\chi_j^+}) \right] \\
&\quad \times (g_{V\chi_j^+\chi_k^-}^R + g_{V\chi_j^+\chi_k^-}^L) (g_{A\chi_k^+\chi_j^-}^R + g_{A\chi_k^+\chi_j^-}^L) \\
F_6^{V,\chi^+} &= \sum_{j,k=1,2} \left[f_6(-m_{\chi_j^+}, -m_{\chi_k^+}, -m_{\chi_k^+}) - g_6(-m_{\chi_k^+}, -m_{\chi_j^+}, -m_{\chi_j^+}) \right] \\
&\quad \times (g_{V\chi_j^+\chi_k^-}^R + g_{V\chi_j^+\chi_k^-}^L) (g_{A\chi_k^+\chi_j^-}^R - g_{A\chi_k^+\chi_j^-}^L)
\end{aligned} \tag{3.43}$$

with $f_{1,3}$ and $g_{1,3}$ given by eqs. (3–14) and the new functions

$$\begin{aligned}
f_6 &= 2m_1(C_0 + C_{11}) \\
g_6 &= 2(m_2C_{11} - m_2C_{12} + m_3C_{12}) .
\end{aligned} \tag{3.44}$$

The arguments of the C_{ij} functions are specified as in eq. (3.15) with $M_\Phi \equiv M_A$.

B. t -channel vertex corrections

The t -channel Aee vertex corrections are built-up only by chargino/sneutrino and neutralino/selectron loops since there is no AVV coupling. Again, these loops do not contribute to $C_{1,2}^e$ and the expression of the contribution to C_3^e is simpler than in the case of the CP-even Higgs bosons, since in the absence of slepton mixing, there is no $A\tilde{l}\tilde{l}$ coupling:

$$\begin{aligned}
C_{1,2}^{e\pm} &= 0 \\
C_3^{e+} &= \frac{e^4}{s_W^3} \left[\sum_{a=R,L} \sum_{j,k} g_{e\chi_j^+\nu} g_{e\chi_k^+\nu} g_{A\chi_j^+\chi_k^-}^a f_{3a}^{ffS}(-m_{\chi_j^+}, m_{\tilde{\nu}}, -m_{\chi_k^+}) \right. \\
&\quad \left. + \frac{1}{2} \sum_{a=R,L} \sum_{j,k} g_{e\chi_j^0\tilde{e}_L} g_{e\chi_k^0\tilde{e}_L} g_{A\chi_j^0\chi_k^0}^a f_{3a}^{ffS}(m_{\chi_j^0}, m_{\tilde{e}_L}, m_{\chi_k^0}) \right] + \text{crossed} \\
C_3^{e-} &= \frac{e^4}{s_W^3} \left[\frac{1}{2} \sum_{a=R,L} \sum_{j,k} g_{e\chi_j^0\tilde{e}_R} g_{e\chi_k^0\tilde{e}_R} g_{A\chi_j^0\chi_k^0}^a f_{3\bar{a}}^{ffS}(m_{\chi_j^0}, m_{\tilde{e}_R}, m_{\chi_k^0}) \right] + \text{crossed}
\end{aligned} \tag{3.46}$$

with the functions f_{3a}^{ffSS} [$\bar{a} = L$ when $a = R$ and vice versa] are given by eq. (3.25) with the same C_{ij} functions as in eq. (3.26) with the replacement $M_\Phi \rightarrow M_A$, and the crossed contributions are obtained by interchanging u and t .

C. Box corrections

Only the chargino/sneutrino and neutralino/selectron boxes contribute to the production of the pseudoscalar. Using the same notation as in the case of the CP-even Higgs bosons, the $C_i^{\text{box}\pm}$ amplitudes are given by

$$\begin{aligned}
C_i^{\text{box}+} &= \frac{e^4}{s_W^3} \left[- \sum_{a=R,L} \sum_{j,k} g_{e\chi_j^+\tilde{\nu}} g_{e\chi_k^+\tilde{\nu}} g_{A\chi_j^+\chi_k^-}^a f_{ia}^{ffSS}(-m_{\chi_j^+}, m_{\tilde{\nu}}, -m_{\chi_k^+}, -m_{\chi_j^+}) \right] + \text{cr.} \\
&\quad + \frac{e^4}{s_W^3} \frac{1}{2} \sum_{a=R,L} \sum_{j,k} g_{e\chi_j^0\tilde{e}_L} g_{e\chi_k^0\tilde{e}_L} g_{A\chi_j^0\chi_k^0}^a g_{ia}^{ffSS}(m_{\chi_j^0}, m_{\tilde{e}_L}, m_{\tilde{e}_L}, m_{\chi_k^0}) \\
C_i^{\text{box}-} &= \frac{e^4}{s_W^3} \frac{1}{2} \sum_{a=R,L} \sum_{j,k} g_{e\chi_j^0\tilde{e}_R} g_{e\chi_k^0\tilde{e}_R} g_{A\chi_j^0\chi_k^0}^a g_{i\bar{a}}^{ffSS}(m_{\chi_j^0}, m_{\tilde{e}_R}, m_{\tilde{e}_R}, m_{\chi_k^0}) \quad (3.47)
\end{aligned}$$

where sums run over the two chargino and the four neutralino states [again $\bar{a} = L, R$ when $a = R, L$]. The various couplings and the box functions f_i^{\dots} and g_i^{\dots} have been given previously eqs. (3.32–3.37); the crossed contribution is obtained by the interchange $u \leftrightarrow t$.

Again, we have checked explicitly that the sum of the contributions $C^e + C^{\text{box}}$ is indeed gauge invariant.

3.3. Results

Before discussing our numerical results, let us first shortly describe our parametrization of the MSSM parameter space. Besides the four masses, M_h, M_H, M_A and M_{H^\pm} , the Higgs sector is described at the tree level by two additional parameters, $\tan\beta$ and a mixing angle α . Due to supersymmetry constraints only two of them are independent and the two inputs are in general taken to be $\tan\beta$ and M_A . Radiative corrections [18, 19], the leading part of which grow as the fourth power of the top mass and logarithmically with the common squark mass, change significantly the relations between masses and couplings and shift the mass of the lightest CP-even Higgs boson upwards. These radiative corrections are very important and should therefore be included in the analysis. We will, however, only include the leading part of this correction which in the simplest case can be parametrized in terms of the quantity [18]

$$\epsilon = \frac{3G_F}{\sqrt{2}\pi^2} \frac{m_t^4}{\sin^2\beta} \log \left(1 + \frac{M_{\tilde{q}}^2}{m_t^2} \right) . \quad (3.48)$$

The CP-even Higgs boson masses are then given in terms of the pseudoscalar mass M_A and $\tan\beta$ as

$$M_{h,H}^2 = \frac{1}{2} \left[M_A^2 + M_Z^2 + \epsilon \right]$$

$$\mp \sqrt{(M_A^2 + M_Z^2 + \epsilon)^2 - 4M_A^2 M_Z^2 \cos^2 2\beta - 4\epsilon(M_A^2 \sin^2 \beta + M_Z^2 \cos^2 \beta)} \Big] \quad (3.49)$$

and the mixing angle α by

$$\tan 2\alpha = \tan 2\beta \frac{M_A^2 + M_Z^2}{M_A^2 - M_Z^2 + \epsilon / \cos 2\beta}, \quad -\frac{\pi}{2} \leq \alpha \leq 0. \quad (3.50)$$

Once $\tan \beta$ and M_A are chosen and the leading radiative correction is included in α and M_h/M_H , all the couplings of the Higgs bosons to fermions, gauge bosons, charginos, neutralinos and sfermions are fixed; these couplings are given in Tables 1 and 2. There is, however, one exception: the trilinear Higgs couplings also receive radiative corrections which are not completely mapped into the corrections to the angle α . The only trilinear couplings which we will need in our analysis are the CP-even Higgs boson couplings to charged Higgs bosons and Goldstones [which are the same at the Born level]; to leading order they are given by [33]

$$\begin{aligned} g_{hH^+H^-} &= \cos 2\beta \sin(\beta + \alpha) + \frac{\epsilon}{M_Z^2} \frac{\cos \alpha \cos^2 \beta}{\sin \beta} \\ g_{HH^+H^-} &= -\cos 2\beta \cos(\beta + \alpha) + \frac{\epsilon}{M_Z^2} \frac{\sin \alpha \cos^2 \beta}{\sin \beta} \\ g_{hG^+G^-} &= \cos 2\beta \sin(\beta + \alpha) + \frac{\epsilon}{M_Z^2} \cos \alpha \sin \beta \\ g_{HG^+G^-} &= -\cos 2\beta \cos(\beta + \alpha) + \frac{\epsilon}{M_Z^2} \sin \alpha \sin \beta \end{aligned} \quad (3.51)$$

It is these expressions which have to be used in order to obtain the same results for the lightest CP-even Higgs boson h and for the SM Higgs boson H^0 in the decoupling limit, and to insure the gauge invariance of the final results.

In the MSSM, there are two charginos $\chi_i^\pm [i = 1, 2]$ and four neutralinos $\chi_i^0 [i = 1-4]$. Their masses and their couplings are given in terms of the Higgs-higgsino mass parameter μ , the ratio of the vacuum expectation values $\tan \beta$ and the wino mass parameter M_2 . The bino and gluino masses are related to M_2 by $M_1 \sim M_2/2$ and $m_{\tilde{g}} \sim 3.5M_2$, when the gaugino masses and the three coupling constants of $SU(3) \times SU(2) \times U(1)$ are unified at the GUT scale. The squark and slepton masses are given in terms of the parameters μ and $\tan \beta$, as well as the left- and right-handed scalar masses $M_{\tilde{f}_L}$ and $M_{\tilde{f}_R}$, which we will take to be equal, and the soft-SUSY breaking trilinear coupling A_f . In the case of the third generation sfermions, mixing between left- and right-handed states is taken into account; in practice it is important only for top squarks.

The total cross sections for the associated production of the lightest CP-even Higgs boson, $e^+e^- \rightarrow h\gamma$, in the unpolarized case are shown in Figs. 4–7. The cross sections for longitudinally polarized electron and positron beams will not be displayed: as in the SM case, they can be obtained by simply rescaling the figures by approximately factor 2 for left-handed electrons and a factor 4 for left-handed electrons and right-handed positrons.

Fig. 4 shows the unpolarized cross sections at a centre of mass energy $\sqrt{s} = 500$ GeV as a function of M_h for two values of $\tan\beta$, $\tan\beta = 2$ and 50. In Fig. 4a(4b), the SUSY parameters have been chosen in such a way that charginos, neutralinos and sleptons will (not) be kinematically reachable at a 500 GeV e^+e^- collider. The solid lines show the total cross sections including the SUSY contributions, while the dashed lines include only the standard and Higgs contributions as it is the case for a two-Higgs doublet model (2HDM) where the MSSM relations have been implemented.

For low M_h the cross sections are smaller than in the SM, especially for large $\tan\beta$ values. This is due to the fact that the main contributions are coming from the W bosons loops, and in the MSSM or 2HDM, the W boson couplings are suppressed by a factor $\sin(\beta - \alpha)$ compared to the SM Higgs coupling. The suppression can be rather drastic, especially for large values of $\tan\beta$, where the cross sections drop to very small values. This can be best seen in Fig. 5 where the cross sections are plotted against $\tan\beta$ for two values of $M_A = 50$ and 500 GeV. With increasing M_h , the cross sections increase and in the 2HDM they reach, as it should be, the SM cross section values in the decoupling limit where M_h is maximal [in practice for $M_A \sim 500$ GeV which leads to $M_h \sim 90$ GeV for $\tan\beta = 2$ and $M_h \sim 120$ GeV for $\tan\beta = 50$].

The contributions of the SUSY particles interfere destructively with the contributions of the standard particles in most of the parameter space. The only exception is when the standard contributions give a very small cross section, as in the case of very high $\tan\beta$ values far from the decoupling limit. In the scenario of Fig. 4a and Fig. 5a, where SUSY particles can be found directly at a c.m. energy of 500 GeV, the difference between the MSSM and the 2HDM is very large, more than a factor of 2. Unfortunately, since the cross section is smaller than in the SM, the signal will be harder to isolate compared to the case of the standard Higgs boson. For the scenario where the SUSY particles are too heavy to be produced directly at the chosen c.m. energy, the SUSY contributions are very small and they will be very difficult to be detected.

This is best illustrated in Fig. 6, where the relative difference between the SM and the MSSM cases in the decoupling limit $M_A \gg M_Z$. In this limit h and the standard H^0 have practically the same couplings and it is very hard to distinguish between the SM and the MSSM. This difference is plotted against M_2 in Fig. 6a and μ in Fig. 6b, for

$\tan\beta = 2, 50$ and for several values of μ and M_2 , respectively. For small values of the parameters M_2 or μ , charginos are light enough to give sizeable contributions, especially near the production threshold. For larger values of these parameters, the SUSY particles are too heavy and since their couplings are not proportional to their masses, they decouple from the production amplitudes rendering the difference between the MSSM and the SM contributions very small.

In Fig. 7, the cross section $e^+e^- \rightarrow h\gamma$ is shown as a function of the c.m. energy for $\tan\beta = 2, 50$ and $M_A = 50$ and 500 GeV. As expected from the SM case, the cross sections decrease smoothly [except when some threshold for the real production of a particle is crossed] with increasing \sqrt{s} . Therefore, to optimize the cross section, one needs to operate the collider at energies around $\sqrt{s} = 200$ GeV. This is about the LEP2 c.m. energy; but at LEP2, the luminosity is so small that no event can be expected.

Finally, Figs. 8 and 9 display the cross sections for the associated production of the heavy CP-even Higgs boson H [Fig. 8] and the pseudoscalar Higgs particle A [Fig. 9] at $\sqrt{s} = 500$ GeV as a function of the Higgs masses. The same scenarios as in Fig. 4 have been chosen. Except for light H and A and for small values of $\tan\beta$, the cross sections are very small. Again, the difference between the MSSM and 2HDM is large only when the SUSY particles are within the reach of the collider.

4. Conclusions

We have calculated the cross sections for the production of Higgs particles in association with a photon in e^+e^- collisions, allowing for the longitudinal polarization of the initial e^- and e^+ beams. We have considered the case of the Standard Model Higgs boson, $e^+e^- \rightarrow \gamma H^0$, and the case of the neutral CP-even and CP-odd Higgs particles of the Minimal Supersymmetric extension of the Standard Model, $e^+e^- \rightarrow \gamma h$, γH and γA . We have given complete and compact analytical expressions, and made careful checks of the gauge invariance of the results, as well as a comparison with earlier results for the associated production of the SM Higgs boson in the case of unpolarized beams.

We have then illustrated the size of the cross sections for energies which will be reached at future e^+e^- colliders. In the SM, the cross sections are in general small but the signals are rather clean. With an integrated luminosity of $\mathcal{L} \sim 100 \text{ fb}^{-1}$ expected at future high-energy e^+e^- colliders and with the polarization of both electron and positron beams, which increase the cross sections by a factor of 4 compared to the unpolarized case, one could hope to isolate the signals despite of the low rates.

The cross sections for the associated production of the lightest MSSM CP-even Higgs

boson are in general smaller than for the SM Higgs boson except in the decoupling limit where they reach the SM values. The contribution of the SUSY particles are significant only when these particles are light enough to be produced directly at the collider. For SUSY particles beyond the reach of the e^+e^- collider, the difference between the SM and MSSM cross sections is very small and will be hard to be detected. For the heavy CP-even and the CP-odd Higgs bosons, the cross sections are rather small especially for large values of $\tan\beta$. Only for small values of $\tan\beta$ and relatively small A and H masses that the cross sections exceed 10^{-2} fb in the unpolarized case.

APPENDIX: Scalar Functions

Our conventions for the scalar Passarino–Veltman functions and for the tensor integrals are as follows [μ is the renormalization scale and D the space–time dimension]

$$\frac{i}{16\pi^2} A(m^2) \equiv \mu^{4-D} \int \frac{d^D k}{(2\pi)^D} \frac{1}{k^2 - m^2} \quad (\text{A.1})$$

$$\frac{i}{16\pi^2} B_0(p_1^2; m_1^2, m_2^2) \equiv \mu^{4-D} \int \frac{d^D k}{(2\pi)^D} \frac{1}{[k^2 - m_1^2][(k + p_1)^2 - m_2^2]} \quad (\text{A.2})$$

$$\begin{aligned} \frac{i}{16\pi^2} C_{0;\mu;\mu\nu}(p_1^2, p_2^2, p_3^2; m_1^2, m_2^2, m_3^2) &\equiv \mu^{4-D} \\ &\int \frac{d^D k}{(2\pi)^D} \frac{1; k_\mu; k_\mu k_\nu}{[k^2 - m_1^2][(k + p_1)^2 - m_2^2][(k + p_1 + p_2)^2 - m_3^2]} \end{aligned} \quad (\text{A.3})$$

$$\begin{aligned} \frac{i}{16\pi^2} D_{0;\mu;\mu\nu}(p_1^2, p_2^2, p_3^2, p_4^2, (p_1 + p_2)^2, (p_2 + p_3)^2; m_1^2, m_2^2, m_3^2, m_4^2) &\equiv \mu^{4-D} \\ &\int \frac{d^D k}{(2\pi)^D} \frac{1; k_\mu; k_\mu k_\nu}{[k^2 - m_1^2][(k + p_1)^2 - m_2^2][(k + p_1 + p_2)^2 - m_3^2][(k + p_1 + p_2 + p_3)^2 - m_4^2]} \end{aligned} \quad (\text{A.4})$$

with the tensor decomposition

$$C^\mu = p_1^\mu C_{11} + p_2^\mu C_{12} \quad (\text{A.5})$$

$$C^{\mu\nu} = p_1^\mu p_1^\nu C_{21} + p_2^\mu p_2^\nu C_{22} + (p_1^\mu p_2^\nu + p_1^\nu p_2^\mu) C_{23} + g^{\mu\nu} C_{24} \quad (\text{A.6})$$

$$D^\mu = p_1^\mu D_{11} + p_2^\mu D_{12} + p_3^\mu D_{13} \quad (\text{A.7})$$

$$\begin{aligned} D^{\mu\nu} &= p_1^\mu p_1^\nu D_{21} + p_2^\mu p_2^\nu D_{22} + p_3^\mu p_3^\nu D_{23} \\ &\quad + (p_1^\mu p_2^\nu + p_1^\nu p_2^\mu) D_{24} + (p_1^\mu p_3^\nu + p_1^\nu p_3^\mu) D_{25} + (p_2^\mu p_3^\nu + p_2^\nu p_3^\mu) D_{26} + g^{\mu\nu} D_{27} \end{aligned} \quad (\text{A.8})$$

The analytical expressions of the scalar functions can be found e.g. in Ref. [28].

Table 1:

g/Φ	h	H	A
$g_{\Phi VV}$	$\sin(\beta - \alpha)$	$\cos(\beta - \alpha)$	0
$g_{\Phi AZ}$	$\cos(\beta - \alpha)$	$-\sin(\beta - \alpha)$	0
$g_{\Phi H^\pm W^\pm}$	$\mp \cos(\beta - \alpha)$	$\pm \sin(\beta - \alpha)$	1
$g_{\Phi G^+ G^-}$	$\cos(2\beta) \sin(\beta + \alpha)$	$\cos(2\beta) \cos(\beta + \alpha)$	0

Tab. 1a: The Higgs–vector boson couplings $g_{\Phi VV}$ [normalized to the SM Higgs coupling $g_{H^0 VV} = 2 \left[\sqrt{2} G_F \right]^{1/2} M_V^2$], and the Higgs–Higgs–vector boson couplings [normalized to $g_W = (\sqrt{2} G_F)^{1/2} M_W$ and $g_Z = (\sqrt{2} G_F)^{1/2} M_Z$ for the charged/neutral weak couplings]; the latter come with the sum of the Higgs momenta entering and leaving the vertices.

Φ	$g_{\Phi \bar{u} u}$	$g_{\Phi \bar{d} d}$
h	$\cos \alpha / \sin \beta$	$-\sin \alpha / \cos \beta$
H	$\sin \alpha / \sin \beta$	$\cos \alpha / \cos \beta$
A	$1 / \tan \beta$	$\tan \beta$

Tab. 1b: Higgs boson couplings in the MSSM to fermions and gauge bosons relative to the SM Higgs couplings.

$g^{L,R}/\Phi$	h	H	A
$g_{\Phi \chi_i^+ \chi_j^-}^L$	$Q_{ji}^* \sin \alpha - S_{ji}^* \cos \alpha$	$-Q_{ji}^* \cos \alpha - S_{ji}^* \sin \alpha$	$-Q_{ji}^* \sin \beta - S_{ji}^* \cos \beta$
$g_{\Phi \chi_i^+ \chi_j^-}^R$	$Q_{ij} \sin \alpha - S_{ij} \cos \alpha$	$-Q_{ij} \cos \alpha - S_{ij} \sin \alpha$	$Q_{ij} \sin \beta + S_{ij} \cos \beta$
$g_{\Phi \chi_i^0 \chi_j^0}^L$	$Q_{ji}''^* \sin \alpha + S_{ji}''^* \cos \alpha$	$-Q_{ji}''^* \cos \alpha + S_{ji}''^* \sin \alpha$	$-Q_{ji}''^* \sin \beta + S_{ji}''^* \cos \beta$
$g_{\Phi \chi_i^0 \chi_j^0}^R$	$Q_{ij}'' \sin \alpha + S_{ij}'' \cos \alpha$	$-Q_{ij}'' \cos \alpha + S_{ij}'' \sin \alpha$	$Q_{ij}'' \sin \beta - S_{ij}'' \cos \beta$

Tab. 1c: The couplings of the neutral Higgs bosons to charginos and neutralinos, normalized to $g_W = \left[\sqrt{2} G_F \right]^{1/2} M_W$; the matrix elements Q_{ij}/S_{ij} and Q_{ij}''/S_{ij}'' can be found in Ref. [31].

Table 2:

\tilde{f}	Φ	g_1^Φ	g_2^Φ	g_3^Φ	g_4^Φ
\tilde{u}	h	$\cos \alpha / \sin \beta$	$-\sin(\alpha + \beta)$	$-\sin \alpha / \sin \beta$	$\cos \alpha / \sin \beta$
	H	$\sin \alpha / \sin \beta$	$\cos(\alpha + \beta)$	$\cos \alpha / \sin \beta$	$\sin \alpha / \sin \beta$
	A	0	0	1	$-1 / \tan \beta$
\tilde{d}	h	$-\sin \alpha / \cos \beta$	$-\sin(\alpha + \beta)$	$\cos \alpha / \cos \beta$	$-\sin \alpha / \cos \beta$
	H	$\cos \alpha / \cos \beta$	$\cos(\alpha + \beta)$	$\sin \alpha / \cos \beta$	$\cos \alpha / \cos \beta$
	A	0	0	1	$-\tan \beta$

Tab. 2a: Coefficients in the couplings of neutral Higgs bosons to sfermion pairs.

$\tilde{l}_i \tilde{l}_j$	$g_{h\tilde{l}_i\tilde{l}_j}$	$g_{H\tilde{l}_i\tilde{l}_j}$	$g_{A\tilde{l}_i\tilde{l}_j}$
$\tilde{e}_L \tilde{e}_L$	$(2s_W^2 - 1) \sin(\beta + \alpha)$	$-(2s_W^2 - 1) \cos(\beta + \alpha)$	0
$\tilde{e}_R \tilde{e}_R$	$2s_W^2 \sin(\beta + \alpha)$	$-2s_W^2 \cos(\beta + \alpha)$	0
$\tilde{\nu}_L \tilde{\nu}_L$	$\sin(\beta + \alpha)$	$-\cos(\beta + \alpha)$	0

Tab. 2b: The couplings of the neutral Higgs bosons to left- and right-handed sleptons in the absence of mixing, normalized to $g'_W = [\sqrt{2}G_F]^{1/2} M_W^2$.

References

- [1] For a review on the Higgs sector of the SM and the MSSM, see J. Gunion, H. Haber, G. Kane and S. Dawson, *The Higgs Hunter's Guide*, Addison–Wesley, Reading 1990.
- [2] For recent discussions of Higgs physics at e^+e^- colliders, see:
Proceedings, *e^+e^- collisions at 500 GeV: The Physics Potential*, Munich–Annecy–Hamburg, DESY 92–123A+C, P.M. Zerwas (ed.);
S. Kuhlman et al., *NLC ZDR Design Group and the NLC Physics Working Group*, Report SLAC-R-0485 (Jun 1996), hep-ex/9605011;
J.F. Gunion, A. Stange and S. Willenbrock, to appear as in a chapter in the *Electroweak Symmetry Breaking and New Physics at the TeV scale*, edited by T.L. Barklow, S. Dawson, H.E. Haber and J.L. Siegrist, World Scientific; hep-ph/9602238;
A. Djouadi, *Int. J. Mod. Phys. A*10 (1995) 1.
- [3] J. Ellis, M.K. Gaillard and D.V. Nanopoulos, *Nucl. Phys. B*106 (1976) 292;
B.W. Lee, C. Quigg and H.H. Thacker, *Phys. Rev. D*16 (1977) 1519;
J.D. Bjorken, *Proc. Summer Inst. on Particle Physics*, SLAC Report 198 (1976);
B. Ioffe and V.A. Khoze, *Sov. J. Part. Nucl.* 9, (1978) 50.
- [4] D.R.T. Jones and S.T. Petcov, *Phys. Lett. B*84 (1979) 440;
R.N. Cahn and S. Dawson, *Phys. Lett. B*136 (1984) 196;
K. Hikasa, *Phys. Lett. B*164 (1985) 341;
G. Altarelli, B. Mele and F. Pitolli, *Nucl. Phys. B*287 (1987) 205;
W. Kilian, M. Krämer and P.M. Zerwas, *Phys. Lett. B*373 (1996) 135.
- [5] M. Hildreth, T.L. Barklow and D.L. Burke, *Phys. Rev. D*49 (1994) 3441.
- [6] A. Djouadi, J. Kalinowski and P. M. Zerwas, *Z. Phys. C*54 (1992) 255.
- [7] K. Hagiwara, H. Murayama and I. Watanabe, *Nucl. Phys. B*367 (1991) 257;
V. Driesen, W. Hollik and A. Kraft, Contribution to the Workshop *Physics with e^+e^- linear Colliders*, 4 Feb - 1 Sep 1995, Report DESY 95–123D, P.M. Zerwas, ed; hep-ph/9603398.
- [8] G. Gounaris, D. Schildknecht and F. Renard, *Phys. Lett. B*83 (1979) 191 and (E) 89B (1980) 437;
V. Barger and T. Han, *Mod. Phys. Lett. A*5 (1990) 667;
A. Djouadi, H. E. Haber and P. M. Zerwas, *Phys. Lett. B*375 (1996) 203;
V. Ilyin, A. Pukhov, Y. Kurihara, Y. Shimitsu and T. Kaneko, KEK CP–030;
F. Boudjema and E. Chopin, Report ENSLAPP–A534/95.

- [9] H.M. Georgi, S.L. Glashow, M.E. Machacek and D.V. Nanopoulos, Phys. Rev.Lett. 40 (1978) 692;
A. Djouadi, M. Spira and P.M. Zerwas, Phys. Lett. B264 (1991) 440;
S. Dawson, Nucl. Phys. B359 (1991) 283;
M. Spira, A. Djouadi, D. Graudenz and P.M. Zerwas, Nucl.Phys. B453 (1995) 17.
- [10] J. Ellis, M.K. Gaillard and D.V. Nanopoulos, Nucl. Phys. B106 (1976) 292;
A. I. Vainshtein et al., Sov. J. Nucl. Phys. 30 (1979) 711.
- [11] L. Bergstrom and G. Hulth, Nucl. Phys. B259 (1985) 137; ERRATUM *ibid* B276 (1986) 744.
- [12] F. Wilczek, Phys. Rev. Lett. 39 (1977) 1304.
- [13] J. F. Gunion and H.E. Haber, Phys. Rev. D48 (1993) 5109;
M. Baillargeon, G. Belanger and F. Boudjema, Phys. Rev. D51 (1995) 4712.
- [14] R.N. Cahn, M.S. Chanowitz, N. Fleishon, Phys. Lett. B82 (1979) 113.
- [15] B. Kniehl, Phys. Rep. 240 (1994) 211.
- [16] See for instance, G. J. Gounaris, F. M. Renard, N. D. Vlachos, Nucl. Phys. B459 (1996) 51.
- [17] H.E. Haber, CERN-TH/95-109 and SCIPP-95/15, Proceedings, *Conference on Physics Beyond the Standard Model IV*, Lake Tahoe CA 1994; and *Perspectives for Electroweak Interactions in e^+e^- Collisions*, Ringberg Castle, Tegernsee 1995.
- [18] Y. Okada, M. Yamaguchi and T. Yanagida, Prog. Theor. Phys. 85 (1991) 1;
H. Haber and R. Hempfling, Phys. Rev. Lett. 66 (1991) 1815;
J. Ellis, G. Ridolfi and F. Zwirner, Phys. Lett. 257B (1991) 83;
R. Barbieri, F. Caravaglios and M. Frigeni, Phys. Lett. 258B (1991) 167.
- [19] R. Hempfling and A. Hoang, Phys. Lett. B331 (1994) 99;
J. Casas, J. Espinosa, M. Quiros and A. Riotto, Nucl. Phys. B436 (1995) 3;
M. Carena, J. Espinosa, M. Quiros and C. Wagner, Phys. Lett. B355 (1995) 209.
- [20] For recent discussions of the Higgs–Photon coupling in the MSSM see: G. L. Kane, G. D. Kribs, S. P. Martin and J. D. Wells, Phys. Rev. D53 (1996) 213;
B. Kileng, P. Osland and P.N. Pandita, Report NORDITA-95-48-P (1995).

- [21] G. Gamberini, G. F. Giudice and G. Ridolfi, Nucl. Phys. B292 (1987) 237;
T. J. Weiler and T. C. Yuan, Nucl. Phys. B318 (1989) 337;
P. Chankowski, S. Pokorski and J. Rosiek, Nucl. Phys. B423 (1994) 437 and Nucl.
Phys. B423 (1994) 497.
- [22] A. Barroso, J. Pulido, J. C. Romao, Nucl. Phys. B267 (1985) 509.
- [23] A. Abbasabadi, D. Bowser-Chao, D. A. Dicus and W. A. Repko, Phys. Rev. D52
(1995) 3919.
- [24] A. Djouadi, V. Driesen and C. Jünger, Phys. Rev. D54 (1996) 759.
- [25] P. Mättig, Report CERN/95–081.
- [26] G. Passarino and M. Veltman, Nucl. Phys. B160 (1979) 151.
- [27] J.A.M. Vermaseren, *Symbolic manipulations with FORM*, 1991, CAN ed;
G.J. Oldenborgh and J.A.M. Vermaseren, Z. Phys. C46 (1990) 425.
- [28] G. 't Hooft and M. Veltman, Nucl. Phys. B153 (1979) 365;
A. Denner, Fortschr. Phys. 41 (1993) 4.
- [29] G.J. Oldenborgh, Comput. Phys. Comm. 66 (1991) 1.
- [30] H.E. Haber, in *Properties of SUSY Particles*, Proceedings of the 23rd Workshop of
the INFN Eloisatron Project, Erice, Italy, 28 September—4 October 1992, edited by
L. Cifarelli and V.A. Khoze (World Scientific, Singapore, 1993) p. 321–372
- [31] H.E. Haber and G. Kane, Phys. Rep. 117 (1985) 75;
J.F. Gunion and H.E. Haber, Nucl. Phys. B272 (1986) 1.
- [32] J. Ellis and S. Rudaz, Phys. Lett. B128 (1983) 248.
- [33] V. Barger, M.S. Berger, A.L. Stange and R.J.N. Phillips, Phys. Rev. D45 (1992)
4128;
A. Brignole and F. Zwirner, Phys. Lett. B299 (1993) 72.

Figure Captions

- Fig. 1:** Feynman diagrams contributing to the process $e^+e^- \rightarrow \gamma H^0$ in the Standard Model (a), the additional diagrams for the production of the MSSM CP-even Higgs bosons $e^+e^- \rightarrow \Phi\gamma$ with $\Phi = h, H$ (b), and of the CP-odd Higgs boson $e^+e^- \rightarrow A\gamma$ (c).
- Fig. 2:** The total cross sections for the production of the Standard Model Higgs boson, $e^+e^- \rightarrow \gamma H^0$, at two center of mass energies $\sqrt{s} = 500$ GeV and $\sqrt{s} = 1.5$ TeV as a function of the Higgs boson mass. The solid, dashed and dotted lines are for the unpolarized, left-handed polarized electrons, and left-handed polarized electrons and right-handed polarized positrons, respectively.
- Fig. 3:** (a) The total production cross section $\sigma(e^+e^- \rightarrow \gamma H^0)$ for unpolarized beams as a function of \sqrt{s} for $M_H = 100$ (solid), 150 (dot-dashed), 200 (dashed) and 300 (dotted) GeV. (b) The differential cross section $d\sigma/d\cos\theta$ at a center of mass energy $\sqrt{s} = 500$ GeV for $M_H = 100$ GeV for unpolarized and polarized e^+e^- beams.
- Fig. 4:** The total cross section for the production of the lightest MSSM Higgs boson, $\sigma(e^+e^- \rightarrow \gamma h)$, in the unpolarized case at $\sqrt{s} = 500$ GeV as a function of M_h for $\tan\beta = 2$ and 50. The solid lines include all MSSM contributions, while the dashed lines include only the contributions from the standard and Higgs sectors (2HDM). For the SUSY parameters we have: in (a) $M_2 = 200$ GeV, $\mu = 200$ GeV, $M_{\tilde{t}} = 200$ GeV, $M_{\tilde{q}} = 500$ GeV, and in (b) $M_2 = 500$ GeV, $\mu = 500$ GeV, $M_{\tilde{t}} = 500$ GeV, $M_{\tilde{q}} = 500$ GeV.
- Fig. 5:** The total production cross section $\sigma(e^+e^- \rightarrow \gamma h)$ for unpolarized beams at $\sqrt{s} = 500$ GeV as a function of $\tan\beta$ for $M_A = 50$ GeV and $M_A = 500$ GeV. The scenarios for the MSSM parameter space are as in Fig. 4.
- Fig. 6:** The difference between the MSSM and the SM cross sections at $\cos\theta = 0$ normalized to the SM values, as a function of the SUSY parameters M_2 and μ for $\tan\beta = 2$ and 50. For the other parameters, we take $M_A = 1$ TeV and $M_{\tilde{q}} = M_{\tilde{t}} = 500$ GeV.
- Fig. 7:** The total production cross section $\sigma(e^+e^- \rightarrow \gamma h)$ as a function of the c.m. energy \sqrt{s} for $M_A = 50$ GeV and $M_A = 500$ GeV and $\tan\beta = 2$ and 50 in the MSSM (solid curves) and in the 2HDM (dashed curves). The SUSY parameters are chosen as: $M_2 = 500$ GeV, $\mu = 500$ GeV, $M_{\tilde{t}} = 500$ GeV and $M_{\tilde{q}} = 500$ GeV.
- Fig. 8:** The total cross section for the production of the heavy CP-even Higgs boson in the MSSM, $\sigma(e^+e^- \rightarrow \gamma H)$, in the unpolarized case at $\sqrt{s} = 500$ GeV as a function of M_H for $\tan\beta = 2$ and 50 in the MSSM (solid curves) and 2HDM (dashed curves). The SUSY parameters are as in Fig. 4.

Fig. 9: The total cross section for the production of the CP-odd Higgs boson in the MSSM, $\sigma(e^+e^- \rightarrow \gamma A)$, in the unpolarized case, at $\sqrt{s} = 500$ GeV as a function of M_A for $\tan \beta = 2$ and 50 in the MSSM (solid) and 2HDM (dashed). The SUSY parameters are as in Fig. 4.

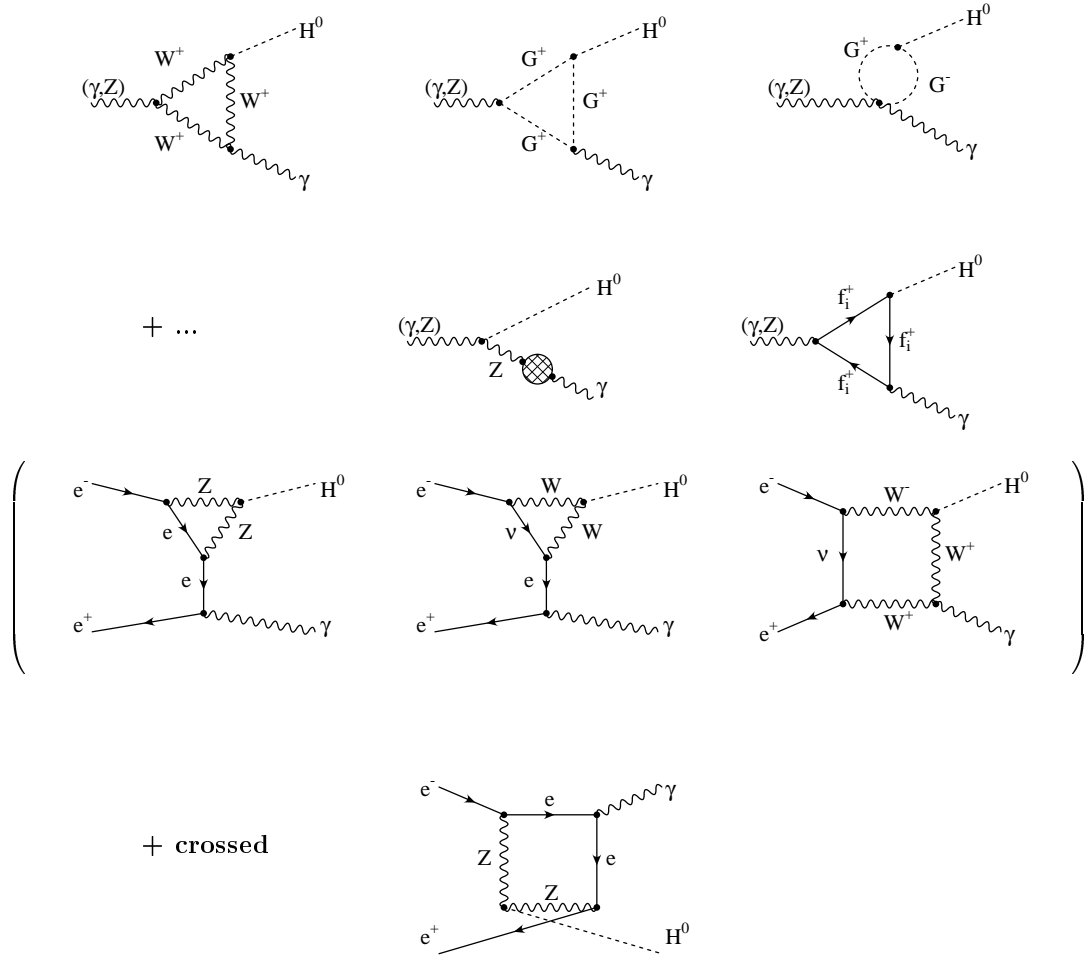
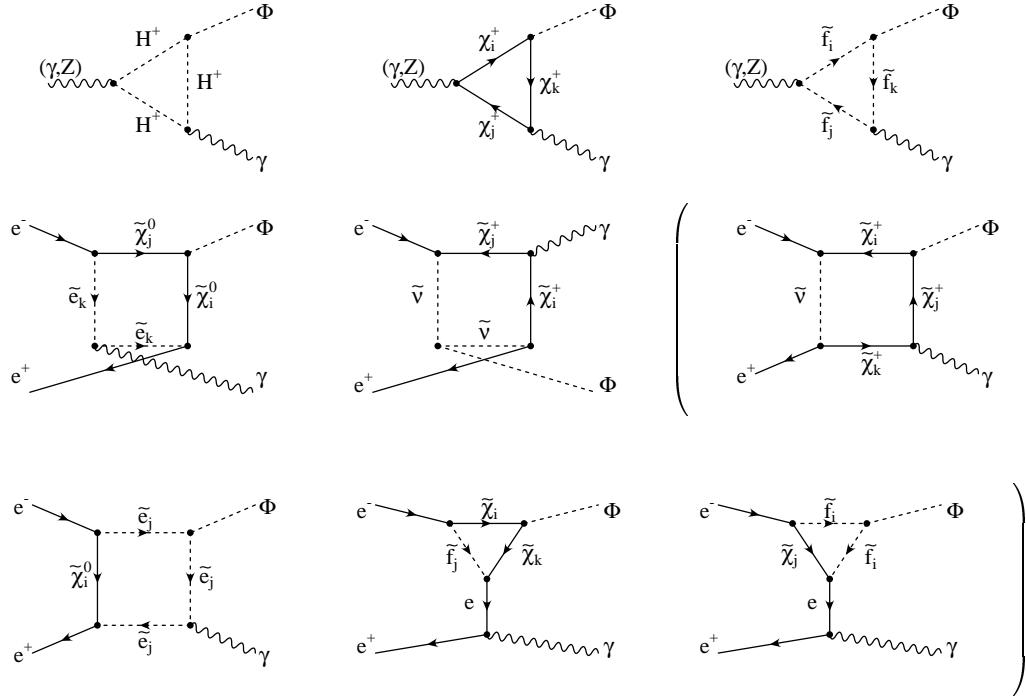
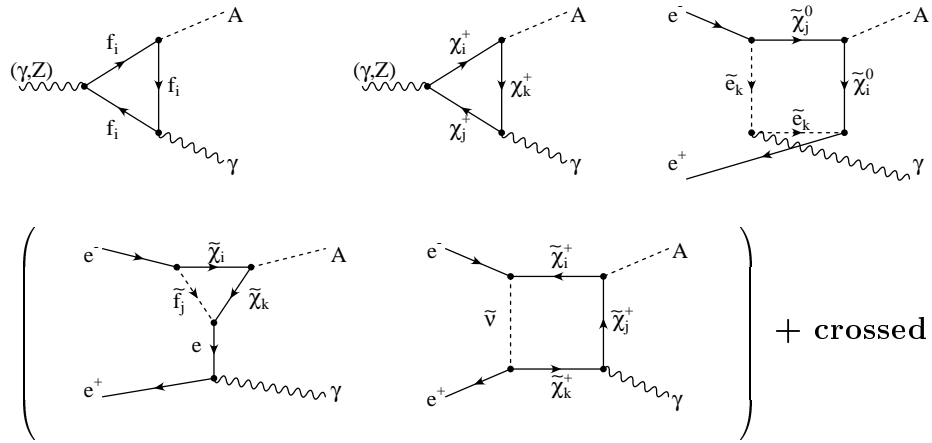


Fig. 1 a



(b)



(c)

Fig. 1

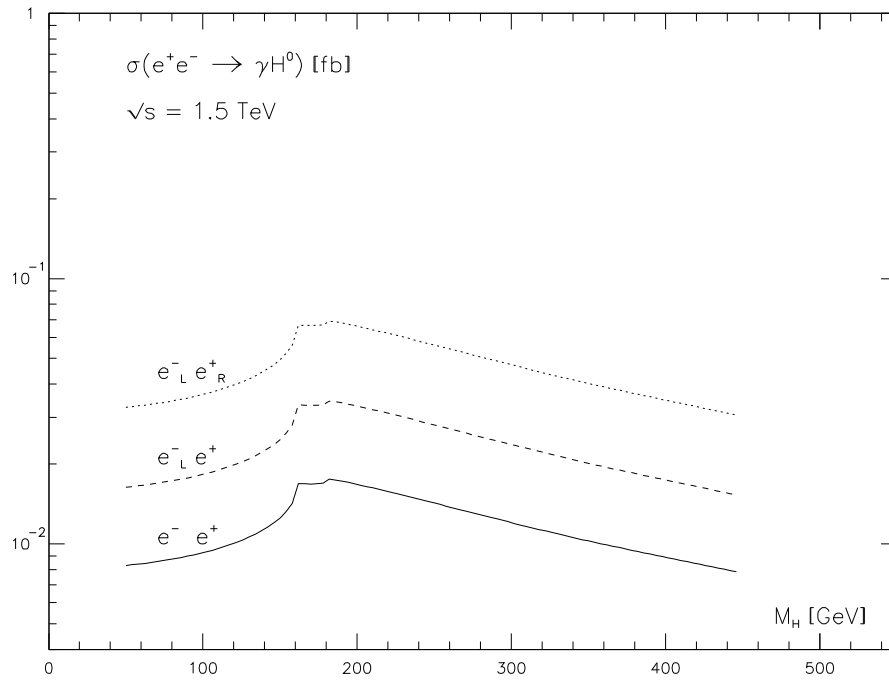
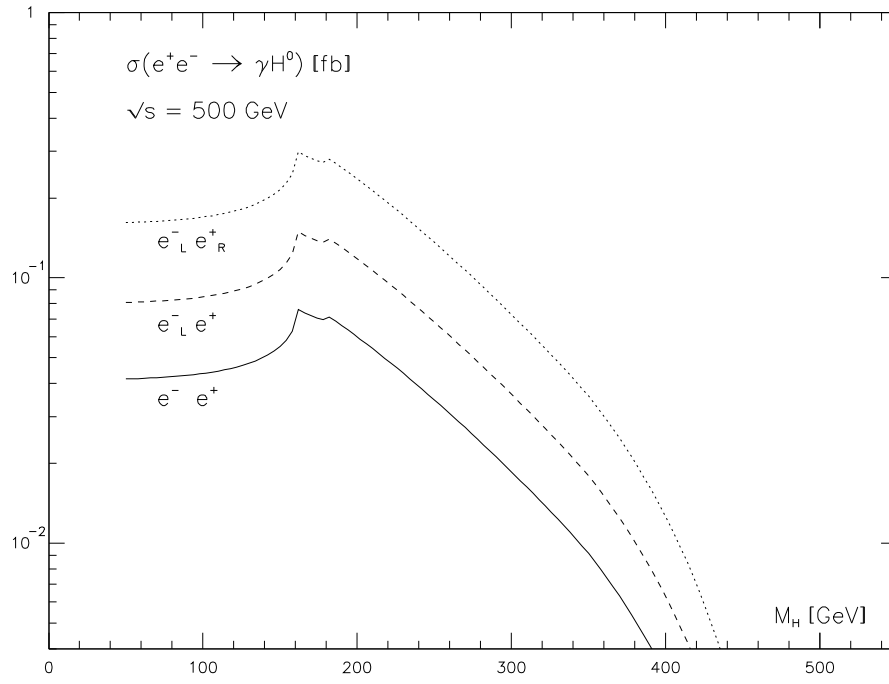


Fig. 2

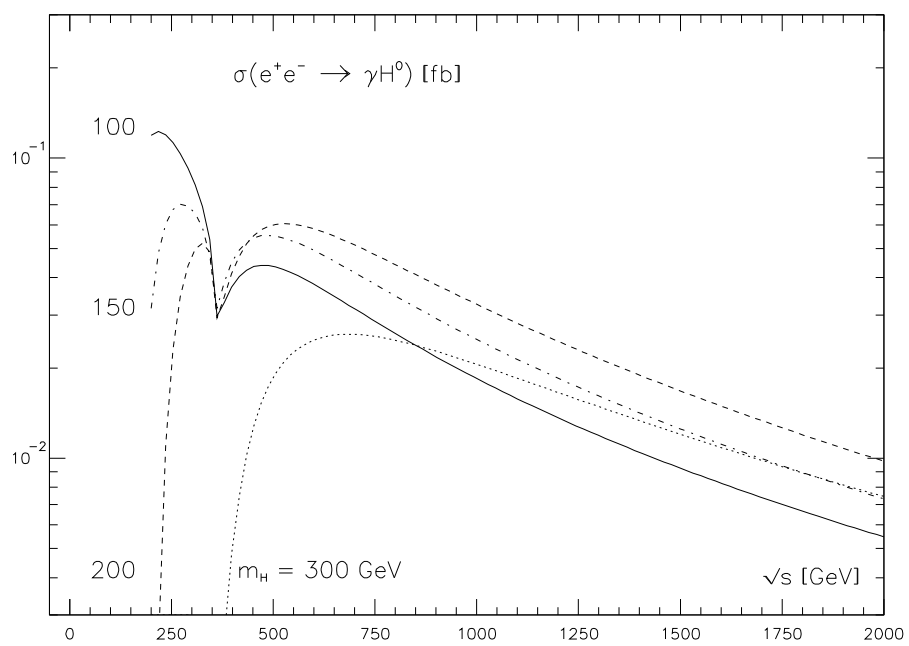


Fig. 3a

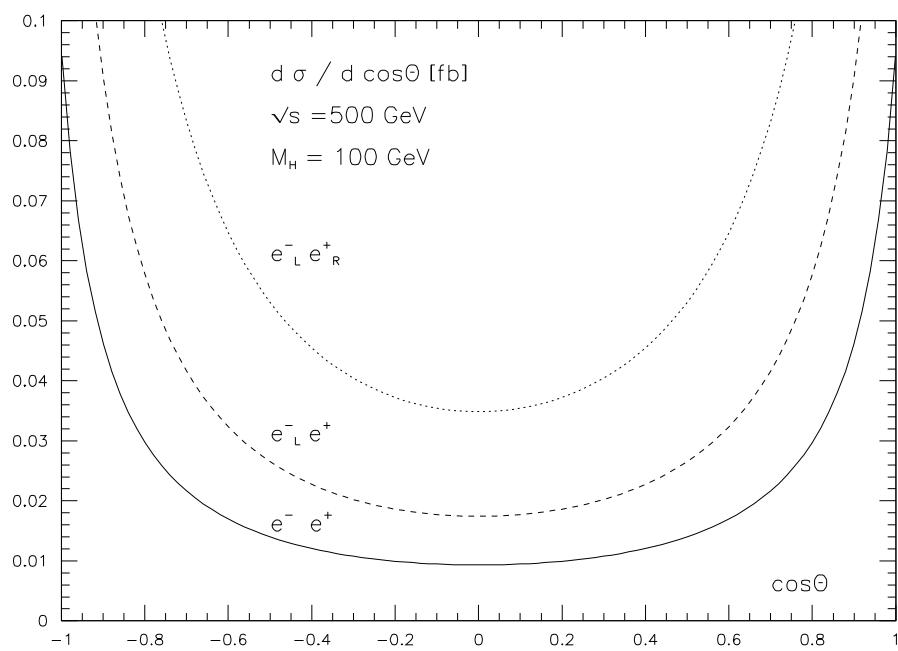


Fig. 3b

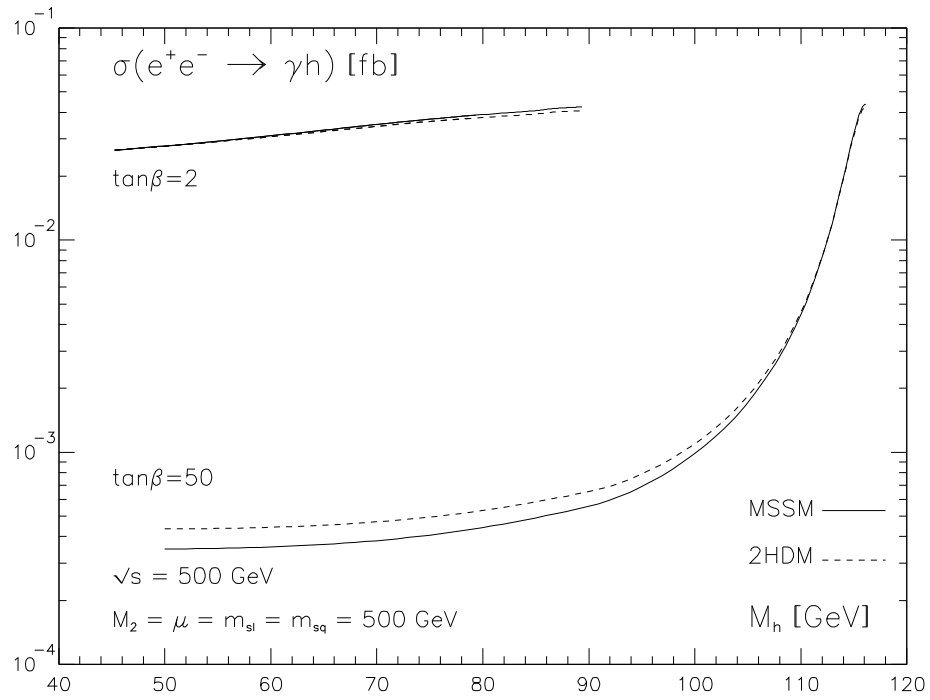
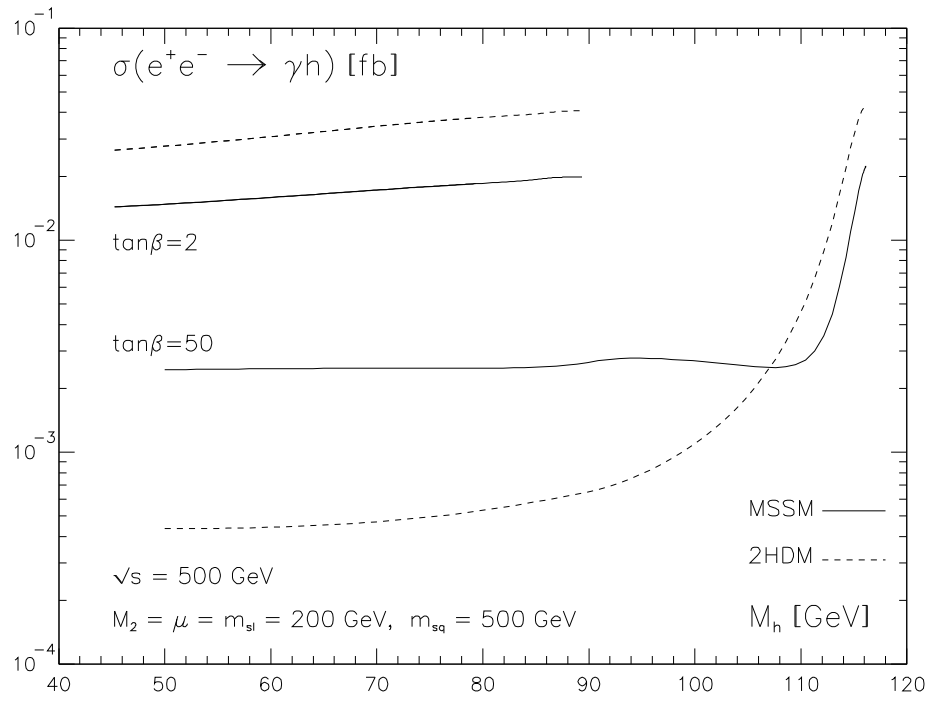


Fig. 4

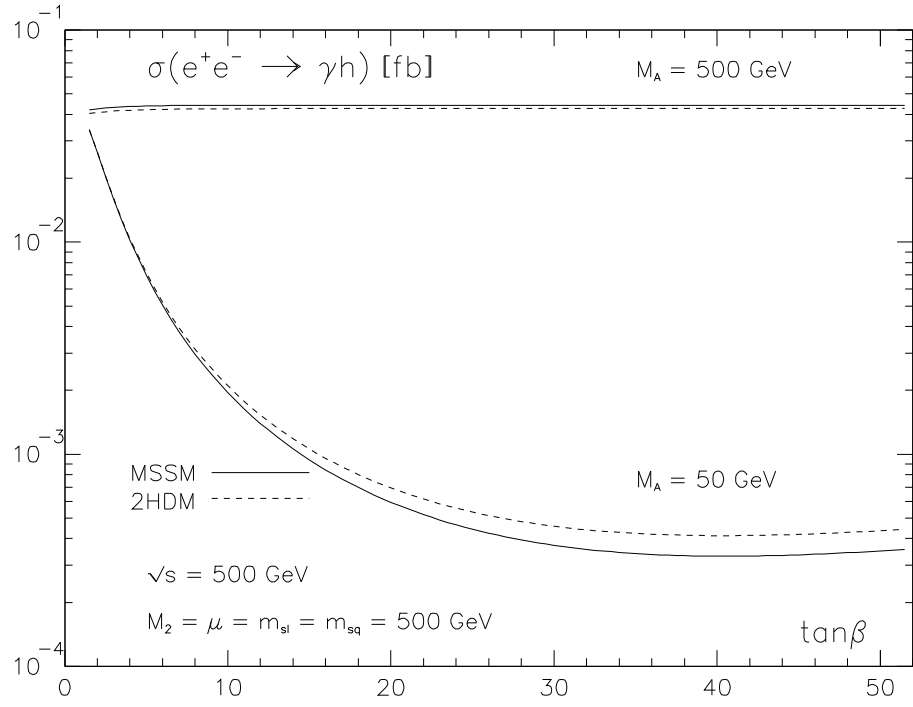
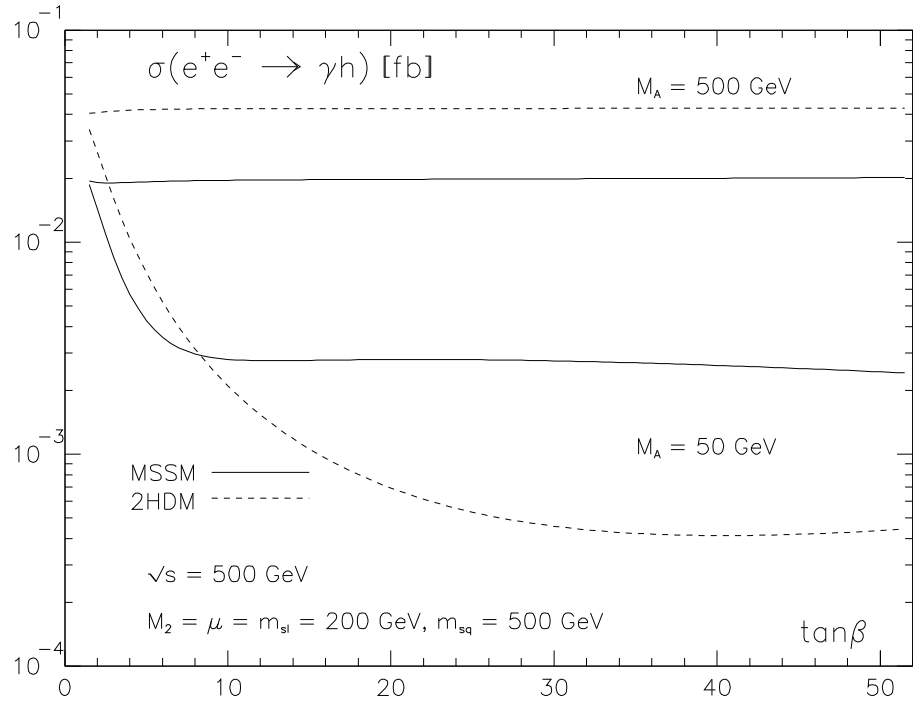


Fig. 5

$$(\mathrm{d}\sigma_{\mathrm{MSSM}} - \mathrm{d}\sigma_{\mathrm{SM}}) / \mathrm{d}\sigma_{\mathrm{SM}} (\cos\Theta=0)$$

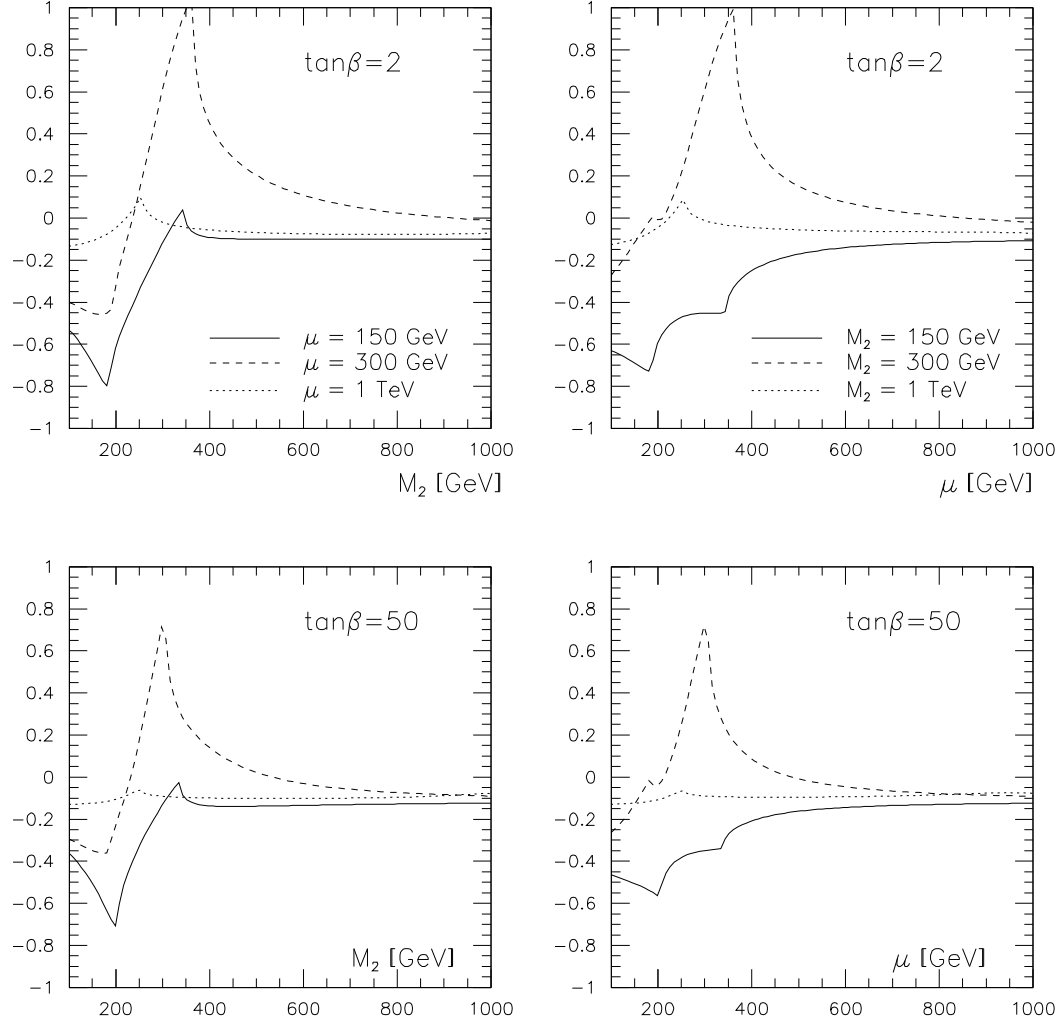


Fig. 6

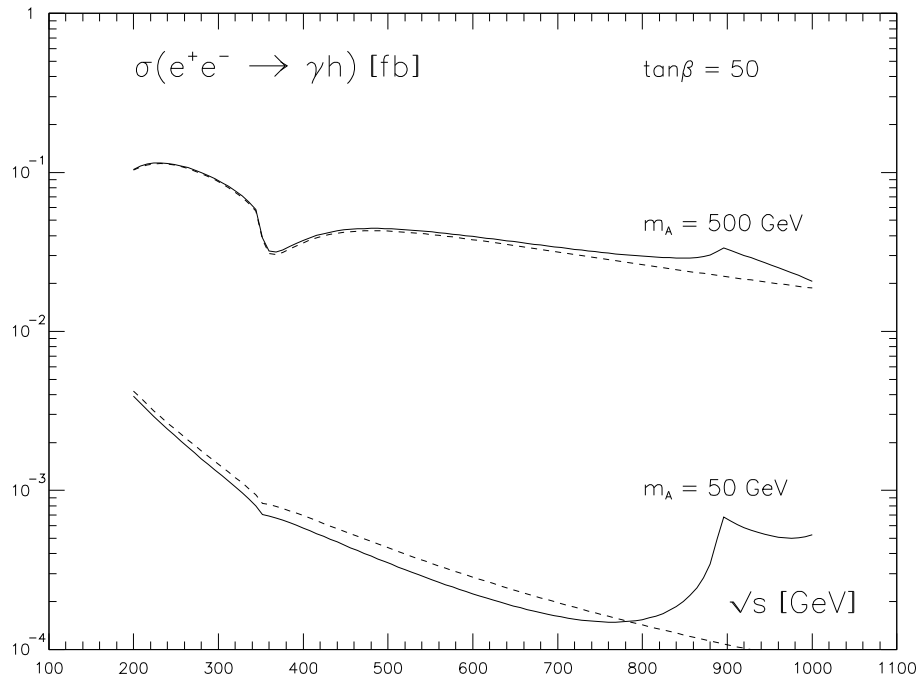
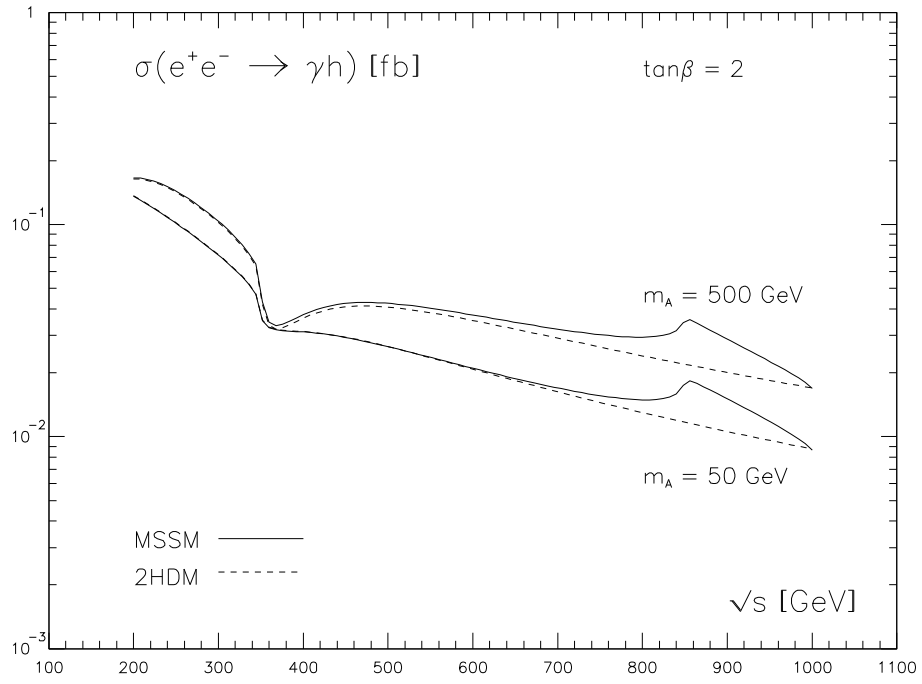


Fig. 7

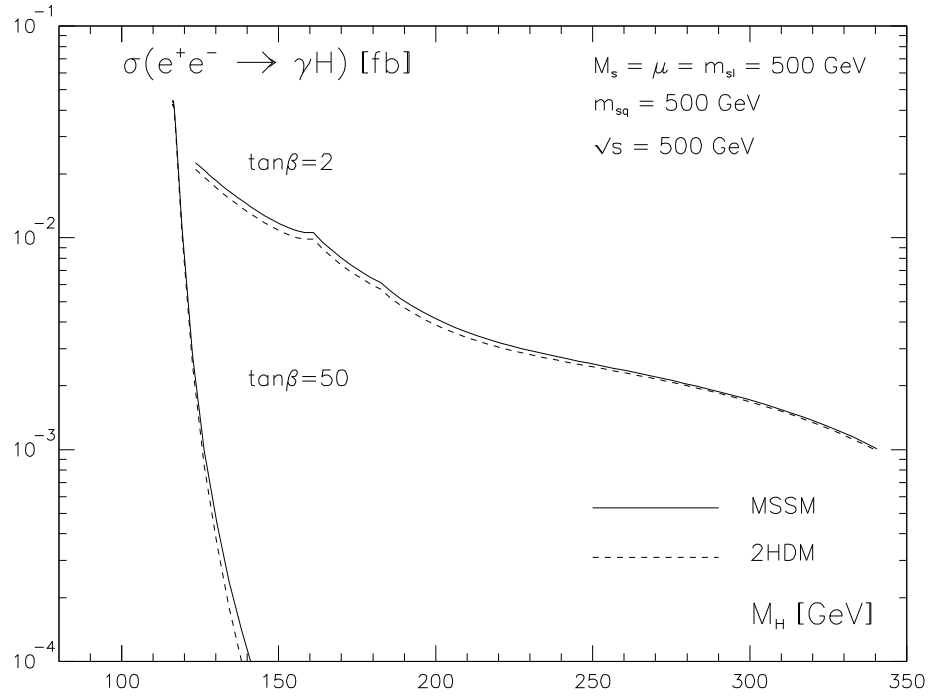
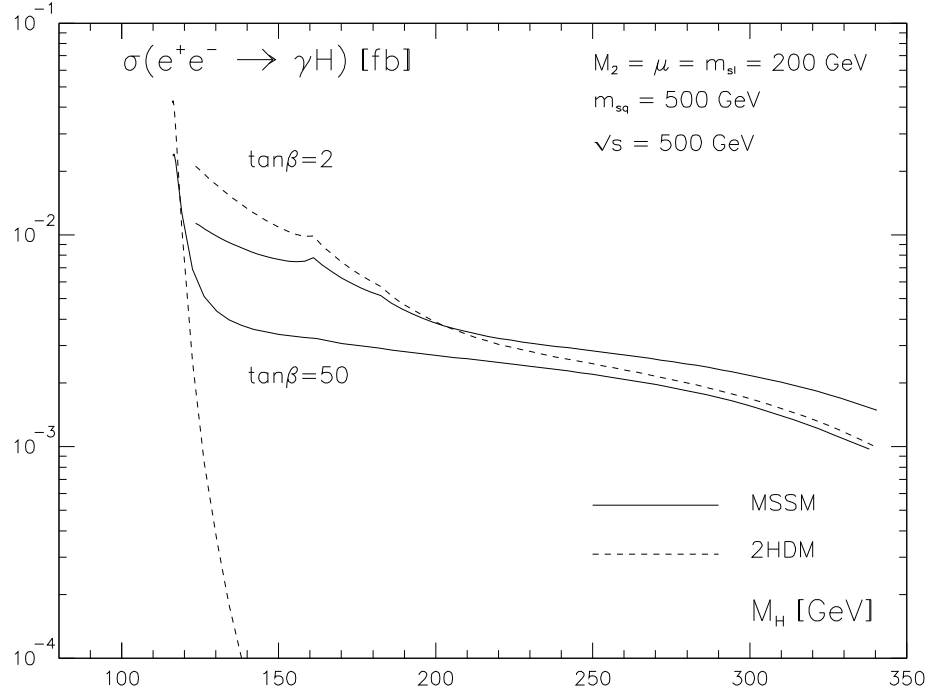


Fig. 8

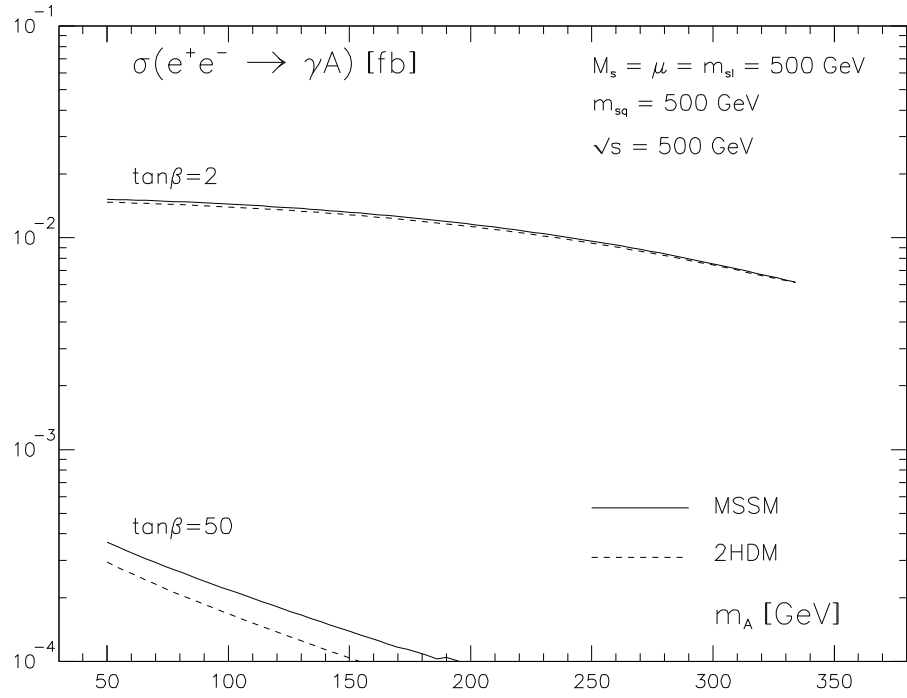
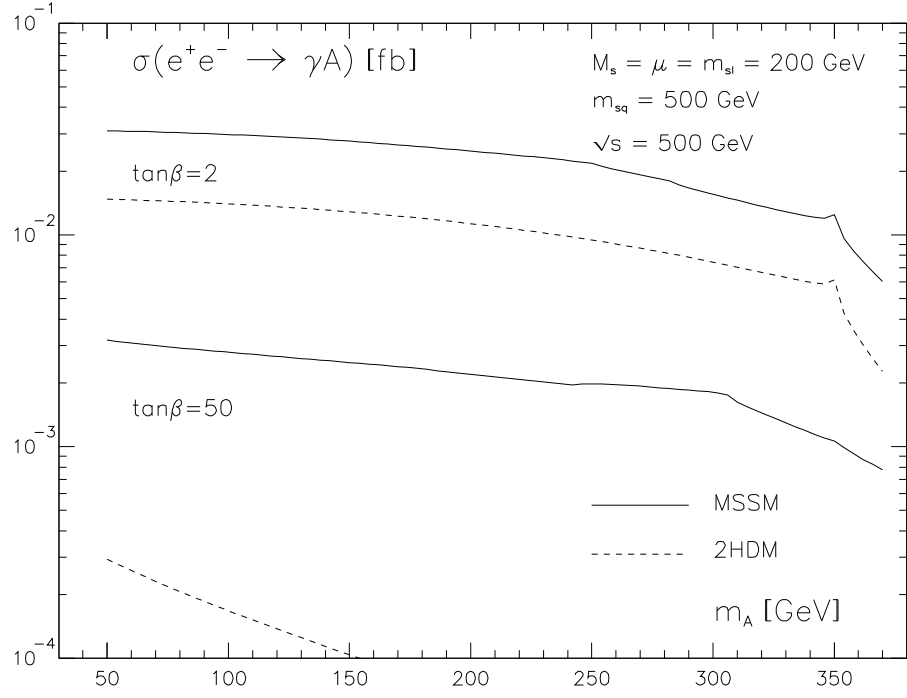


Fig. 9